JOC Article
pubs.acs.org/joc

Synthesis and Reactions of Phosphaporphyrins: Reconstruction of π-Skeleton Triggered by Oxygenation of a Core Phosphorus Atom

Takashi Nakabuchi,[†] Makoto Nakashima,[†] Shinya Fujishige,[‡] Haruyuki Nakano,[‡] Yoshihiro Matano,*[,†] and Hiroshi Imahori[†,§,⊥]

[†]*Department of Molecular Engineering, Graduate School of Engineering, Kyoto University, Nishikyo-ku, Kyoto 615-8510, Japan,* [‡]*Department of Chemistry, Graduate School of Sciences, Kyushu University, Fukuoka 812-8581, Japan,* [§]*Institute for Integrated Cell-Material Sciences (iCeMS), Kyoto University, Nishikyo-ku, Kyoto 615-8510, Japan, and* [⊥]*Fukui Institute for Fundamental Chemistry, Kyoto University, Sakyo-ku, Kyoto 606-8103, Japan*

matano@scl.kyoto-u.ac.jp

Received October 7, 2009

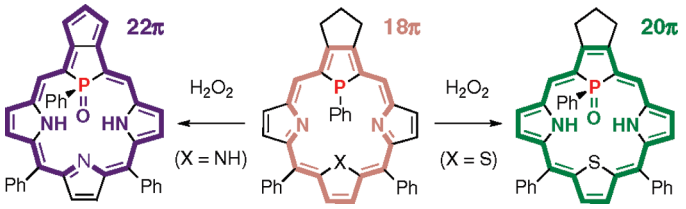

The synthesis, structures, optical and redox properties, and reactivity of phosphaporphyrins are reported. The 21-phosphaporphyrin (P,N_3-porphyrin) and 23-phospha-21-thiaporphyrin (P,S,N_2-porphyrin) were prepared via acid-promoted dehydrative condensation between a phosphatripyrrane and the corresponding 2,5-bis[hydroxy(phenyl)methyl]heteroles followed by 2,3-dichloro-5,6-dicyanobenzoquinone oxidation. Experimental (NMR, UV−vis, and X-ray analyses) and theoretical (DFT calculations) results suggest that the 18π aromaticity inherent in regular N_4-porphyrins was maintained in these phosphaporphyrins. X-ray crystallography revealed a slightly distorted 18π aromatic ring for the P,N_3-porphyrin with the phosphole and three pyrrole rings tilted from the 24-atoms mean plane by 9.6° and 3.8−15.4°, respectively. DFT calculations on model compounds showed that the P,X,N_2-porphyrins (X = N, S) possess considerably small HOMO−LUMO gaps as compared with N_4- and S,N_3-porphyrins, which is reflected in the red-shifted absorptions, low oxidation potentials, and high reduction potentials of the phosphaporphyrins. The P-oxygenation of the P,X,N_2-porphyrins with H_2O_2 has been found to lead to the formation of different types of products. The 18π P,N_3-porphyrin was transformed into the 22π aromatic P(O),N_3-porphyrin accompanied by the π extension at the peripheral C_3 bridge, whereas the 18π P,S,N_2-porphyrin was converted to the isophlorin-type 20π antiaromatic P(O),S,N_2-porphyrin. In both of the reactions, simple P-oxygenated 18π P(O),X,N_2-porphyrins were formed as the initial products, which were subsequently transformed into the 22π or 20π porphyrins. The two reaction courses from 18π to 20π/22π are apparently determined by the combination of the core heteroatoms (i.e., P,N_3 or P,S,N_2) and the structure of the peripherally fused carbocycles. The present results demonstrate that the incorporation of a phosphorus atom into the core is not only a highly promising way to modify the fundamental properties of the porphyrin 18π system but also a reliable tool to stabilize uncommon 22π and 20π systems through the chemical modifications at the core phosphorus atom.

Introduction

Porphyrins are one of the most widely studied macrocyclic heterocycles because of their important roles in biological and materials chemistry. To perturb optical, electrochemical, and coordinating properties of porphyrins, chemical modifications of the macrocyclic platform have generally been employed. Core modification, namely, the replacement

DOI: 10.1021/jo902060b Published on Web 12/14/2009

of one or more core nitrogen atoms by other heteroatoms or carbon, is a highly promising chemical modification methodology.[1−5] Recent extensive studies on core-modified porphyrins have disclosed that the electronic structures of their π circuits differ significantly from those of regular porphyrins (hereafter denoted as the N_4-porphyrins). For instance, Soret and Q bands of 21-chalcogena- and 21,23-dichalcogenaporphyrins are red-shifted from those of N_4-porphyrins, and the bathochromic shifts of these heteroporphyrins are strongly dependent on the relevant core chalcogens (O, S, Se, Te).[2f] The incorporation of four chalcogens (O, S) at the core has been successfully utilized to stabilize planar 20π systems (isophlorin skeletons) that are difficult to construct with N_4-porphyrins.[6] An additional promising aspect of the core-modified porphyrins is the unique reactivity endowed by the core elements. For example, the 21-tellurapoprhyrins undergo the Te−O exchange reaction[7] or oxidative chlorination[8] at the tellurium center via Te-oxygenation, and carbaporphyrinoids, typically in their metal complex forms, exhibit a variety of reactivities such as alkylation,[9] cyanization,[10] diphenylphosphanylation,[11] halogenation,[12] nitration,[12] oxygenation,[13] pyridination,[14] and internal fusion.[12] Despite these encouraging findings on the core-modified porphyrins, the types of elements introduced into the core have been limited to carbon, silicon,[15] and chalcogens. Under these circumstances, we were interested in the chemistry of phosphaporphyrin, a heavy analogue of the parent N_4-porphyrin, because the phosphole subunit provides unprecedented optical, electrochemical, and coordinating properties to the porphyrin platform.

In sharp contrast to pyrrole, phosphole forms a trigonal pyramid structure at the phosphorus center and behaves basically as a neutral P ligand and as a highly conjugative *cis*-1,3-dienic π system.[16] Such structural and electronic properties of phosphole are beneficial for the construction of an unprecedented class of core-modified porphyrins. Most importantly, the tricoordinate (σ^3) phosphorus center can be converted to various tetracoordinate (σ^4) forms by simple chemical modification such as P-oxygenation (to σ^4-P=O), P-thioxygenation (to σ^4-P=S), and P-metal coordination (to σ^4-P−metal) with its active lone electron pair.[17] This implies that the electronic structure of a phosphaporphyrin π system is readily tunable by the introduction of P substituents.

In 2003, Delaere and Nguyen predicted the electronic structures and optical properties of unsubstituted 21-phospha- and 21,23-diphosphaporphyrins based on density functional theory (DFT) calculations and concluded that these phosphaporphyrins would exhibit reasonable aromaticity.[18] However, the synthesis of phosphaporphyrins has not been reported until recently, presumably due to the lack of their potential precursors. The reactivity of phosphole is well-known to arise from the low aromatic character of the five-membered ring and the high nucleophilicity of the σ^3-phosphorus atom. Accordingly, conventional methods (Friedel−Crafts alkylation and direct lithiation) that have

(1) For reviews, see: (a) Latos-Grażyński, L. In *The Porphyrin Handbook*; Kadish, K. M., Smith, K. M., Guilard, R., Eds.; Academic Press: San Diego, 2000; Vol 2, Chapter 14. (b) Furuta, H.; Maeda, H.; Osuka, A. *Chem. Commun*. **2002**, 1795–1804. (c) Srinivasan, A.; Furuta, H. *Acc. Chem. Res*. **2005**, *38*, 10–20. (d) Chandrashekar, T. K.; Venkatraman, S. *Acc. Chem. Res*. **2003**, *36*, 676–691. (e) Stepień, M.; Latos-Grażyński, L. *Acc. Chem. Res*. **2005**, *38*, 88–98. (f) Chmielewski, P. J.; Latos-Grażyński, L. *Coord. Chem. Rev*. **2005**, *249*, 2510–2533. (g) Gupta, I.; Ravikanth, M. *Coord. Chem. Rev*. **2006**, *250*, 468–518. (h) Lash, T. D. *Eur. J. Org. Chem*. **2007**, 5461–5481. (i) Misra, R.; Chandrashekar, T. K. *Acc. Chem. Res*. **2008**, *41*, 265–279.

(2) Chalcogen-containing porphyrins. For example, see: (a) Broadhurst, M. J.; Grigg, R.; Johnson, A. W. *J. Chem. Soc. C* **1971**, 3681–3690. (b) Ulman, A.; Manassen, J. *J. Am. Chem. Soc*. **1975**, *97*, 6540–6544. (c) Latos-Grażyński, L.; Lisowski, J.; Olmstead, M. M.; Balch, A. L. *J. Am. Chem. Soc*. **1987**, *109*, 4428–4429. (d) Chmielewski, P. J.; Latos-Grażyński, L.; Olmstead, M. M.; Blalch, A. L. *Chem.−Eur. J*. **1997**, *3*, 268–278. (e) Sridevi, B.; Narayanan, S. J.; Srinivasan, A.; Chandrashekar, T. K.; Subramanian, J. *J. Chem. Soc., Dalton Trans*. **1998**, 1979–1984. (f) Abe, M.; Hilmey, D. G.; Stilts, C. E.; Sukumaran, D. K.; Detty, M. R. *Organometallics* **2002**, *21*, 2986–2992. (g) Agarwal, N.; Ravikanth, M. *Tetrahedron* **2004**, *60*, 4739–4747. (h) Uno, H.; Shimizu, Y.; Uoyama, H.; Tanaka, Y.; Okujima, T.; Ono, N. *Eur. J. Org. Chem*. **2008**, 87–98. (i) Cho, D.-G.; Plitt, P.; Lim, S. K.; Lynch, V.; Hong, S,-J.; Lee, C.-H.; Sessler, J. L. *J. Am. Chem. Soc*. **2008**, *130*, 10502–10503.

(3) Carbaporphyrinoids. For example, see: (a) Berlin, K.; Breitmaier, E. *Angew. Chem., Int. Ed. Engl*. **1994**, *33*, 1246–1247. (b) Berlin, K. *Angew. Chem., Int. Ed. Engl*. **1996**, *35*, 1820–1822. (c) Lash, T. D.; Hayes, M. J. *Angew. Chem., Int. Ed. Engl*. **1997**, *36*, 840–842. (d) Stepień, M.; Latos-Grażyński, L. *Chem.−Eur. J*. **2001**, *7*, 5113–5117. (e) Lash, T. D.; Hayes, M. J.; Spence, J. D.; Muckey, M. A.; Ferrence, G. M.; Szczepura, L. F. *J. Org. Chem*. **2002**, *67*, 4860–4874. (f) Sprutta, N.; Swiderska, M.; Latos-Grażyński, L. *J. Am. Chem. Soc*. **2005**, *127*, 13108–13109.

(4) N-Confused porphyrins. For example, see: (a) Furuta, H.; Asano, T.; Ogawa, T. *J. Am. Chem. Soc*. **1994**, *116*, 767–768. (b) Chmielewski, P. J.; Latos-Grażyński, L.; Rachlewicz, K.; Glowiak, T. *Angew. Chem., Int. Ed. Engl*. **1994**, *33*, 779–781. (c) Furuta, H.; Maeda, H.; Osuka, A. *J. Am. Chem. Soc*. **2000**, *122*, 803–807. (d) Furuta, H.; Ishizuka, T.; Osuka, A. *J. Am. Chem. Soc*. **2002**, *124*, 5622–5623. (e) Morimoto, T.; Uno, H.; Furuta, H. *Angew. Chem., Int. Ed*. **2007**, *46*, 3672–3675. (f) Toganoh, M.; Kimura, T.; Furuta, H. *Chem.−Eur. J*. **2008**, *14*, 10585–10594.

(5) Pyriporphyrins. For example, see: (a) Berlin, K.; Breitmaier, E. *Angew. Chem., Int. Ed. Engl*. **1994**, *33*, 219–220. (b) Lash, T. D.; Chaney, S. T. *Chem.−Eur. J*. **1996**, *2*, 944–948. (c) Mysliborski, R.; Latos-Grażyński, L.; Szterenberg, L. *Eur. J. Org. Chem*. **2006**, 3064–3068. (d) Sim, E.-K.; Jeong, S.-D.; Yoon, D.-W.; Hong, S.-J.; Kang, Y.; Lee, C.-H. *Org. Lett*. **2006**, *8*, 3355–3358. (e) Lash, T. D.; Pokharel, K.; Serling, J. M.; Yant, V. R.; Ferrence, G. M. *Org. Lett*. **2007**, *9*, 2863–2866.

(6) Chalcogen-containing isophlorins: (a) Pohl, M.; Schmickler, H.; Lex, J.; Vogel, E. *Angew. Chem., Int. Ed. Engl*. **1991**, *30*, 1693–1697. (b) Reddy, J. S.; Anand, V. G. *J. Am. Chem. Soc*. **2008**, *130*, 3718–3719.

(7) Latos-Grażyński, L.; Pacholska, E.; Chmielewski, P. J.; Olmstead, M. M.; Blalch, A. L. *Angew. Chem., Int. Ed. Engl*. **1995**, *34*, 2252–2254.

(8) Abe, M.; Detty, M. R.; Gerlits, O. O.; Sukumaran, D. K. *Organometallics* **2004**, *23*, 4513–4518.

(9) (a) Chmielewski, P. J.; Latos-Grażyński, L.; Glowiak, T. *J. Am. Chem. Soc*. **1996**, *118*, 5690–5701. (b) Schmidt, I.; Chmielewski, P. J. *Inorg. Chem*. **2003**, *42*, 5579–5593.

(10) Xiao, Z.; Patrick, B. O.; Dolphin, D. *Chem. Commun*. **2003**, 1062–1063.

(11) Grzegorzek, N.; Pawlicki, M.; Szterenberg, L.; Latos-Grażyński, L. *J. Am. Chem. Soc*. **2009**, *131*, 7224–7225.

(12) Furuta, H.; Ishizuka, T.; Osuka, A.; Ogawa, T. *J. Am. Chem. Soc*. **2000**, *122*, 5748–5757.

(13) (a) Hung, C.-H.; Chen, W.-C.; Lee, G.-H.; Peng, S.-M. *Chem. Commun*. **2002**, 1516–1517. (b) Xiao, Z.; Patrick, B. O.; Dolphin, D. *Inorg. Chem*. **2003**, *42*, 8125–8127. (c) Stepień, M.; Latos-Grażyński, L.; Szterenberg, L. *J. Org. Chem*. **2007**, *72*, 2259–2270. (d) Lash, T. D.; Szymanski, J. T.; Ferrence, G. M. *J. Org. Chem*. **2007**, *72*, 6481–6492.

(14) Stepień, M.; Latos-Grażyński, L. *Org. Lett*. **2003**, *5*, 3379–3381.

(15) Latos-Grażyński and co-workers attempted to synthesize 21-silaporphyrin, which led them to the serendipitous discovery of a unique transformation of 21-silaphlorin into a carbacorrole. Skonieczny, J.; Latos-Grażyński, L.; Szterenberg, L. *Chem.−Eur. J*. **2008**, *14*, 4861–4874.

(16) For reviews, see: (a) Mathey, F. *Chem. Rev*. **1988**, *88*, 429–453. (b) Quin, L. D. In *Comprehensive Heterocyclic Chemistry II*; Katritzky, A. R., Rees, C. W., Scriven, E. F. V., Eds.; Elsevier: Oxford, 1996; Chapter 15. (c) Hissler, M.; Dyer, P. W.; Réau, R. *Coord. Chem. Rev*. **2003**, *244*, 1–44. (d) Mathey, F. *Angew. Chem., Int. Ed*. **2003**, *42*, 1578–1604. (e) Baumgartner, T.; Réau, R. *Chem. Rev*. **2006**, *106*, 4681−4727; (correction) **2007**, *107*, 303. (f) Hobbs, M. G.; Baumgartner, T. *Eur. J. Inorg. Chem*. **2007**, *23*, 3611–3628. (g) Réau, R.; Dyer, P. W. In *Comprehensive Heterocyclic Chemistry III*; Ramsden, C. A., Scriven, E. F. V., Taylor, R. J. K., Eds.; Elsevier: Oxford, 2008; Chapter 3.15. (h) Matano, Y.; Imahori, H. *Org. Biomol. Chem*. **2009**, *7*, 1258–1271.

(17) For example, see: (a) Hay, C.; Hissler, M.; Fischmeister, C.; Rault-Berthelot, J.; Toupet, L.; Nyulászi, L.; Réau, R. *Chem.−Eur. J*. **2001**, *7*, 4222–4236. (b) Delaere, D.; Nguyen, M. T.; Vanquickenborne, L. G. *J. Phys. Chem. A* **2003**, *107*, 838–846. (c) Baumgartner, T.; Bergmans, W.; Kárpáti, T.; Neumann, T.; Nieger, M.; Nyulászi, L. *Chem.−Eur. J*. **2005**, *11*, 4687–4699.

(18) Delaere, D.; Nguyen, M. T. *Chem. Phys. Lett*. **2003**, *376*, 329–337.

CHART 1. (a) 21-Phospha- and 21,23-Diphosphaporphyrins Calculated by Delaere and Nguyen. (b) Mathey's P-Confused Carbaporphyrinoid

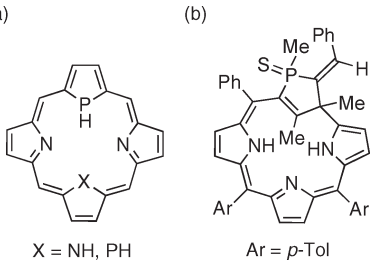

been widely used for the α-functionalization of pyrrole and thiophene are not applicable to phosphole. Recently, Mathey's group and our group independently reported convenient methods for the synthesis of 2,5-difunctionalized phospholes based on sequential [1,5]-sigmatropic shifts in P-functionalized phospholes[19] and Ti^{II}-mediated cyclization of difunctionalized diynes,[20] respectively. 2,5-Bis[hydroxymethyl]-type phospholes, suitable starting materials of phosphaporphyrins, are now readily available in gram scale.

In 2007, Mathey and co-workers reported an attempt to prepare a phosphaporphyrin via acid-promoted [3 + 1] condensation of a 2,5-bis[phenyl(hydroxy)methyl]phosphole, where the phosphorus atom was masked as the σ^4-P=S form, with a tripyrrane. However, this approach resulted in the formation of a small amount of "P-confused" carbaporphyrinoid (Chart 1).[21,22] In 2006, we reported the first synthesis of a phosphaporphyrin of the P,S,N_2-type. This synthesis was achieved by using a different [3 + 1] condensation approach starting from a phosphatripyrrane (vide infra),[23a] and this method was later applied to the synthesis of a P,N_3-type phosphaporphyrin.[23b] With these encouraging results available, we aimed to uncover the structures, aromaticity, and optical/electrochemical properties of phosphaporphyrins by comparison with those of known porphyrins. We also aimed to clarify the reactivities of phosphaporphyrins, especially those at the core phosphorus atom, as well as the fundamental properties of the resulting P-functionalized

CHART 2. Phosphaporphyrins 1N and 1S and Thiaporphyrins 2N and 2S

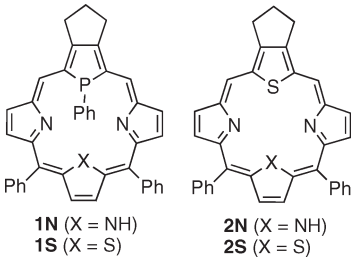

derivatives. We envisioned that these comparative studies would highlight the characteristics of phosphorus in porphyrin chemistry and heteroatom chemistry.

In this report, full details of the synthesis and reactions of 21-phosphaporphyrin (P,N_3-porphyrin) **1N** and 23-phospha-21-thiaporphyrin (P,S,N_2-porphyrin) **1S** (Chart 2) are described.[23,24] The structures, aromaticity, and optical/electrochemical properties of **1N**, **1S**, and their P-functionalized derivatives are discussed in detail. The replacement of the N−H unit of the N_4-porphyrin with the P−Ph unit induced dramatic alternations in the fundamental properties and reactivity of the porphyrin ring. In particular, these 18π phosphaporphyrins underwent unique π-reconstructions triggered by P-oxygenation, resulting in the formation of 22π or 20π systems depending on the combination of the core heteroatoms and the structure of the peripherally fused carbocycles.[25]

Results and Discussion

1. Synthesis and Characterization of Phosphaporphyrins. 1.1. Synthesis. Scheme 1 illustrates the synthesis of 21-phosphaporphyrin **1N** and 23-phospha-21-thiaporphyrin **1S**. The BF_3-promoted dehydrative condensation of P-masked phosphatripyrrane **3**[23a] with 2,5-bis[hydroxy(phenyl)methyl]-pyrrole **4N**,[26] -thiophene **4S**,[2b] or -furan **4O**[2d] afforded P-masked P,X,N_2-porphyrinogens **5X**−**S** (X = N, S, O) in 9−43% yields as a mixture of two or three diastereomers. Desulfurization of **5X**−**S** with excess $P(NMe_2)_3$ in refluxing toluene produced the corresponding σ^3-P,X,N_2-porphyrinogens **5X** (X = N, S, O) in good yields. Compounds **5X** were subsequently treated with 3.3 equiv of 2,3-dichloro-5,6-dicyanobenzoquinone (DDQ) at room temperature. In the DDQ oxidation of **5N**, two major products were obtained. Flash column chromatography of the crude reaction mixture on alumina (CH_2Cl_2/hexane = 1/1) followed by recrystallization from MeOH gave a reddish purple solid (R_f = 0.9) and a dark-purple solid (R_f = 0.5) in 17% and 8% yields, respectively. On the basis of the spectroscopic and crystallographic analyses (vide infra), the less polar compound was characterized as the expected 21-phosphaporphyrin **1N**, whereas the more polar compound was found to be the P-oxo-type phosphaporphyrin **6**−**O**. Under similar conditions, **5S** reacted with DDQ to afford two major products. Flash column chromatography of the

(19) (a) Holand, S.; Jeanjean, M.; Mathey, F. *Angew. Chem., Int. Ed. Engl.* **1997**, *36*, 98–100. (b) Toullec, P; Mathey, F. *Synlett* **2001**, 1977–1979.

(20) Matano, Y.; Miyajima, T.; Nakabuchi, T.; Matsutani, Y.; Imahori, H. *J. Org. Chem.* **2006**, *71*, 5792–5795.

(21) Duan, Z.; Clochard, M.; Donnadieu, B.; Mathey, F.; Tham, F. S. *Organometallics* **2007**, *26*, 3617–3620.

(22) Mathey and co-workers prepared some phosphole-containing macrocycles: (a) Laporte, F.; Mercier, F.; Ricard, L.; Mathey, F. *J. Am. Chem. Soc.* **1994**, *116*, 3306–3311. (b) Deschamps, E.; Ricard, L.; Mathey, F. *J. Chem. Soc., Chem. Commun.* **1995**, 1561. (c) Mercier, F.; Laporte, F.; Ricard, L.; Mathey, F.; Schröder, M.; Regitz, M. *Angew. Chem., Int. Ed. Engl.* **1997**, *36*, 2364–2366.

(23) For preliminary results, see: (a) Matano, Y.; Nakabuchi, T.; Miyajima, T.; Imahori, H.; Nakano, H. *Org. Lett.* **2006**, *8*, 5713–5716. (b) Matano, Y.; Nakashima, M.; Nakabuchi, T.; Imahori, H.; Fujishige, S.; Nakano, H. *Org. Lett.* **2008**, *10*, 553–556.

(24) Recently we reported phosphole-containing calixpyrroles and calixphyrins: (a) Matano, Y.; Nakabuchi, T.; Miyajima, T.; Imahori, H. *Organometallics* **2006**, *25*, 3105–3107. (b) Matano, Y.; Miyajima, T.; Nakabuchi, T.; Imahori, H.; Ochi, N.; Sakaki, S. *J. Am. Chem. Soc.* **2006**, *128*, 11760–11761. (c) Matano, Y.; Miyajima, T.; Ochi, N.; Nakabuchi, T.; Shiro, M.; Nakao, Y.; Sakaki, S.; Imahori, H. *J. Am. Chem. Soc.* **2008**, *130*, 990−1002; (correction) **2009**, *131*, 14123. (d) Nakabuchi, T.; Matano, Y.; Imahori, H. *Organometallics* **2008**, *27*, 3142–3152. (e) Matano, Y.; Imahori, H. *Acc. Chem. Res.* **2009**, *42*, 1193–1204. (f) Matano, Y.; Fujita, M.; Miyajima, T.; Imahori, H. *Phosphorus, Sulfur Silicon Relat. Elem.* In press. (g) Matano, Y.; Fujita, M.; Miyajima, T.; Imahori, H. *Organometallics* **2009**, *28*, 6213–6217.

(25) Recently, we found that **1S** undergoes redox-coupled complexation with zero-valent group 10 metals (M = Ni, Pd, Pt) to afford air-stable M^{II}-P,S,N_2-isophlorin complexes: Matano, Y.; Nakabuchi, T.; Fujishige, S.; Nakano, H.; Imahori, H. *J. Am. Chem. Soc.* **2008**, *130*, 16446–16447.

(26) Heo, P.-Y.; Lee, C.-H. *Bull. Korean Chem. Soc.* **1996**, *17*, 515–520.

SCHEME 1. Synthesis of P,X,N_2-Porphyrins

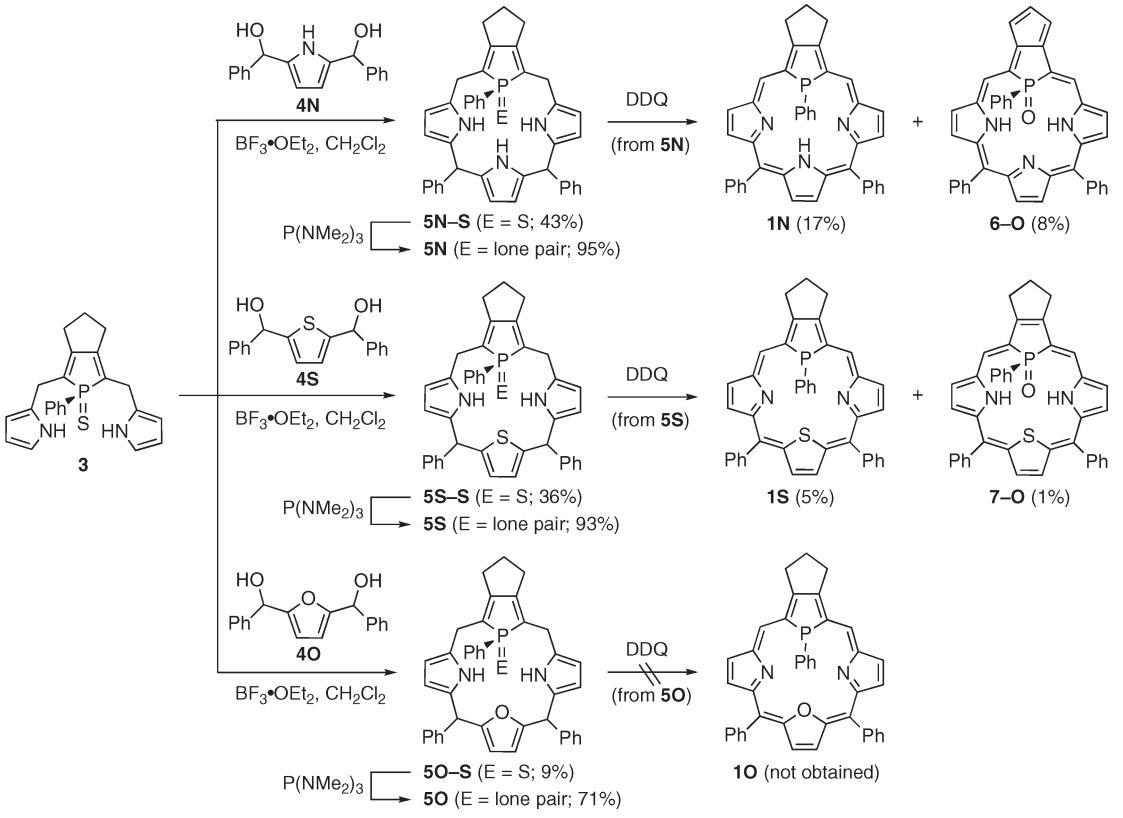

SCHEME 2. Synthesis of P,N_3-Porphyrin Bearing a Peripheral C_4-Bridge

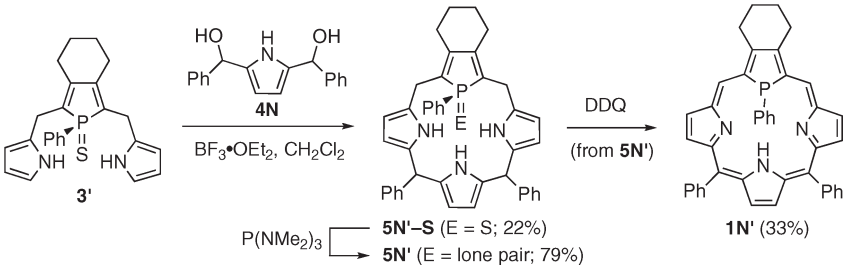

crude reaction mixture on alumina (CH_2Cl_2/hexane = 1/1) followed by recrystallization from MeOH gave reddish purple (R_f = 0.7) and dark-green (R_f = 0.9) solids in 5% and 1% yields, respectively. In this case, the more polar compound was found to be the expected 23-phospha-21-thiaporphyrin **1S**, and the less polar compound was the P-oxo derivative **7**−**O**.[27] Although the isolated yields of the products were low, the formation of **1X**, **6**−**O**, and **7**−**O** was quite reproducible. Unfortunately, all attempts to prepare 21-phospha-23-oxaporphyrin **1O** from **5O** were unsuccessful; DDQ oxidation of **5O** resulted in the formation of a complex mixture. Another P,N_3-porphyrin, **1N′**, which bears a peripheral C_4-bridge at the phosphole ring, was also prepared from the corresponding precursors **3′** and **4N** (Scheme 2). In this case, the P-oxo byproducts like **6**−**O** were not obtained. All of the phosphaporphyrins **1N**, **1N′**, and **1S** were observed to be stable in the solid state but slowly decomposed in solution under aerobic conditions and in room light. We assume that **6**−**O** and **7**−**O** were mainly formed by the P-oxidation of the corresponding P,X,N_2-porphyrins **1N** and **1S** during the reaction conditions employed. The details of these reactions will be discussed later.

To compare core-modification effects on the fundamental properties of porphyrin π systems, 21-thia- and 21,23-dithiaporphyrins, **2N** and **2S**[25] (Chart 2), were newly prepared by a similar [3 + 1]-type condensation of thiatripyrrane **S2** with **4X** (X = N, S) followed by DDQ oxidation (Scheme S1 in Supporting Information). In the synthesis of **2X**, no S-oxo (sulfoxide or sulfone) type byproducts were produced.

1.2. Characterization. The diagnostic spectral features of P,X,N_2-porphyrins **1N**, **1N′**, and **1S** are as follows. In the high-resolution FAB-MS (HR-FAB-MS) spectra, the parent ion peaks (M^+) were observed at m/z 595.2182 for **1N** (calcd for $C_{41}H_{30}N_3P$, 595.2177), 609.2335 for **1N′** (calcd for $C_{42}H_{32}N_3P$, 609.2334), and 612.1788 for **1S** (calcd for $C_{41}H_{29}N_2PS$, 612.1789). In the ^{1}H NMR spectrum of **1N**, *meso* and pyrrole-β protons appeared at δ 10.18

(27) After the preliminary results were published (ref 23a), we noticed that a small amount of **7**−**O** was also isolable beside **1S**.

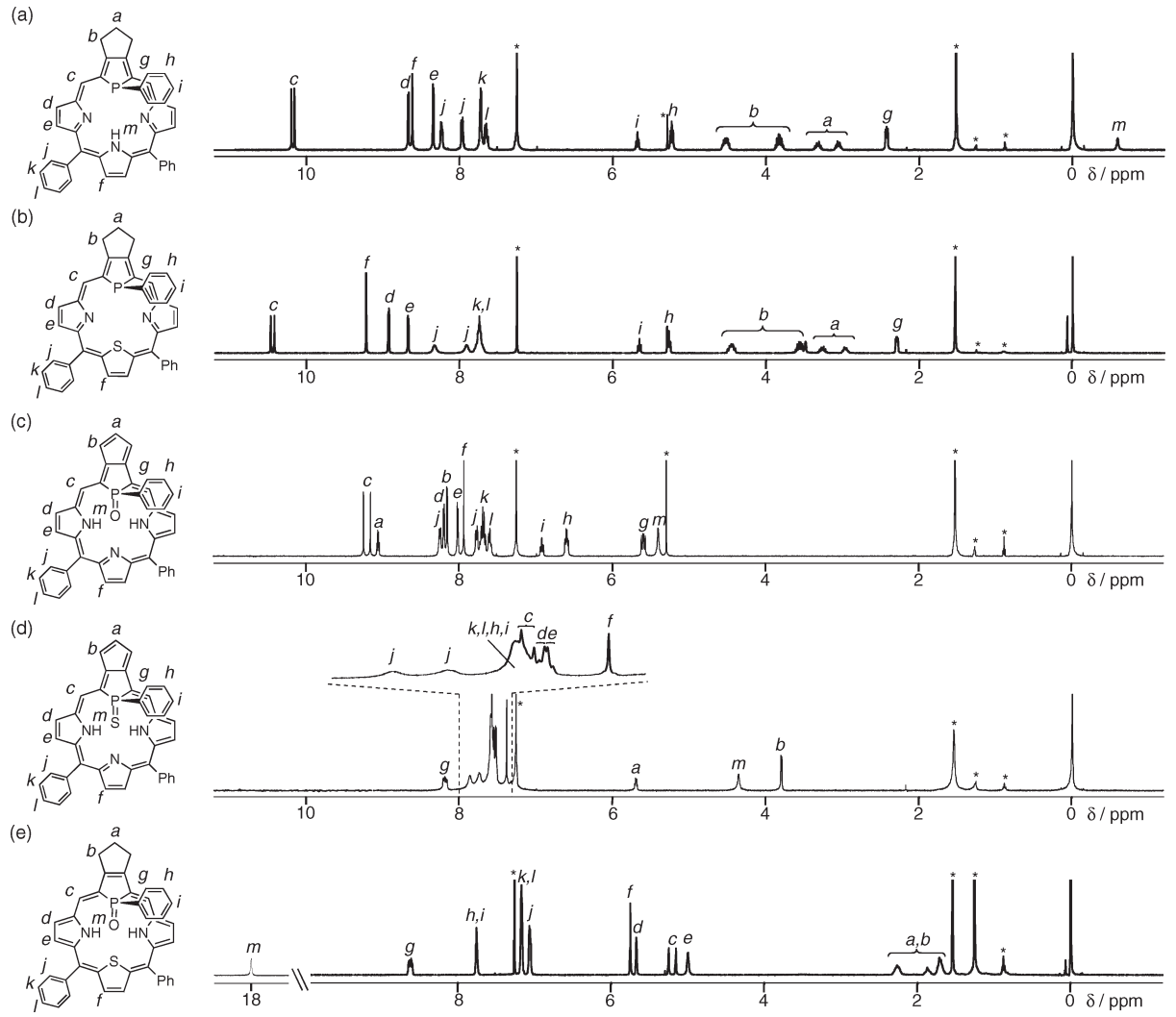

FIGURE 1. ^{1}H NMR spectra of phosphaporphyrins (a) **1N**, (b) **1S**, (c) **6**−**O**, (d) **6**−**S**, and (e) **7**−**O** in $CDCl_3$. Asterisks (∗) indicate the peaks of residual solvents.

(d, $^{3}J_{P,H}$ = 16.1 Hz) and 8.35−8.67 ppm, respectively, whereas the NH and P-phenyl protons appeared at δ −0.59 and 2.43−5.68 ppm, respectively (Figure 1a; Table S1 in Supporting Information). It is apparent that the significant downfield and upfield positions of these peaks stem from ring current effects of the porphyrin 18π-electron circuit. In the ^{1}H NMR spectra of **1N′** and **1S** (Figure 1b), similar diatropic ring current effects were observed. To evaluate and compare the ring current effects quantitatively, the difference in chemical shifts ($\Delta\delta$) of the heterole-β and P-phenyl protons between **1X** (X = N, S) and calixphyrins **8X** (X = N, S)[24b,c] (Chart 3) was used as an index. As the π circuits in **8X** are interrupted at the sp^{3}-hybridized *meso* carbons, the positive/negative signs and the absolute values of $\Delta\delta$ (Table 1) represent the diatropicity (paratropicity) and the degree of the aromaticity (antiaromaticity) of the π-circuits of **1X**. The downfield shifts of the heterole-β protons observed for the S,X,N_2-porphyrins **2X** (X = N, S) versus the S,X,N_2-calixphyrins **9X** (X = N, S)[28] are also summarized in Table 1.

The data for the heterole-β protons indicate that the ring current effects increase in the order S_2,N_2-porphyrin > P,S,N_2-porphyrin ≈ S,N_3-porphyrin > P,N_3-porphyrin. The diminished ring current effects in the P,X,N_2-porphyrins as compared with the corresponding S,X,N_2-porphyrins may be ascribed to the slightly deviated π-planes in the phosphaporphyrins (vide infra). The upfield shifts of the P-phenyl protons of **1X** versus **8X** increase in the order *ortho* > *meta* > *para*, implying that the P-phenyl group in **1X** stands above the porphyrin π-plane. As summarized in Table S1 in Supporting Information, the ring current effects also emerged as upfield positions of the ^{31}P peaks of **1N** (δ −5.2 ppm), **1N′** (δ −32.6 ppm), and **1S** (δ 18.6 ppm) relative to the ^{31}P peaks of the respective precursors, **5N** (δ 30.4−32.7 ppm), **5N′** (δ 2.6−4.1 ppm), and **5S** (δ 32.7−33.5 ppm).[29] The structural and spectral properties of the P-oxo porphyrins **6**−**O** and **7**−**O** will be summarized later.

(28) Matano, Y.; Miyajima, T.; Ochi, N.; Nakao, Y.; Sakaki, S.; Imahori, H. *J. Org. Chem.* **2008**, *73*, 5139–5142.

(29) Phosphorus-31 chemical shifts of phospholes are sensitive to the substituents on the phosphorus atom and β-carbons. Since we have no data about ^{31}P chemical shifts of P-oxo calixphyrins and the C_4-bridge type calixphyrins, the ^{31}P chemical shifts of the C_n-bridge type P(E),X,N_2-porphyrins (n = 3, 4; E = lone pair, O, S; X = N, S) are compared with those of the corresponding porphyrinogens.

CHART 3. P,X,N_2-Calixphyrins 8X, 8X−S, and 14 and S,X, N_2-Calixphyrins 9X (X = N, S)

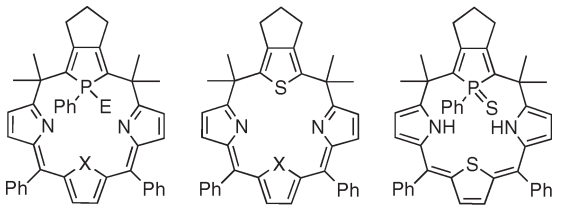

8N (X = NH, E = lone par) **9N** (X = NH) **14**
8S (X = S, E = lone par) **9S** (X = S)
8N–S (X = NH, E = S)
8S–S (X = S, E = S)

TABLE 1. Differences in the ^{1}H NMR Chemical Shifts ($\Delta\delta$, ppm) between Porphyrins and Calixphyrins[a]

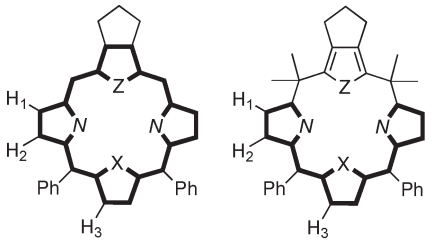

porphyrins calixphyrins

porphyrin/calixphyrin	heterole-β (β_1, β_2, β_3)	P-Ph (*ortho*, *meta*, *para*)
1N/**8N**	+2.08, +1.79, +2.70	−5.1, −2.0, −1.6
1N′/**8N**	+1.93, +1.65, +2.53	−5.0, −2.1, −2.0
1S/**8S**	+2.29, +2.07, +2.62	−5.3, −2.0, −1.6
2N/**9N**	+2.29, +1.97, +2.89	
2S/**9S**	+2.35, +2.13, +3.10	
6−O/**8N−S**	+1.56, +1.48, +1.98	−2.5, −0.9, −0.6
6−S/**8N−S**	+0.90, +0.97, +1.42	+0.1, +0.1, +0.1
7−O/**14**	−0.35, −0.97, −0.76	+0.7, +0.5, +0.6

[a]Measured in $CDCl_3$. Chemical shifts for the calixphyrin references were reported in ref 24b, 24c (for **8X**, **8X−S**, and **14**) and ref 28 (for **9X**). $\Delta\delta = \delta$ (porphyrin) − δ (calixphyrin). The plus sign indicates a downfield shift and the minus sign indicates an upfield shift.

The structure of **1N** was unambiguously determined by X-ray crystallography.[23b] The selected bond lengths and distances are summarized in Table 2. The porphyrin ring in **1N** is slightly distorted, wherein the phosphole and three pyrrole rings are tilted from the 24-atom mean plane with dihedral angles of 9.6° and 3.8−15.4°, respectively. The differences between the contiguous carbon(*meso*)−carbon-(α) bond lengths (i.e., the absolute values of $d-c$ and $k-j$ in Table 2) are notably suppressed (0.03−0.04 Å), which indicates the efficient π-electron delocalization through the 18π circuit of **1N**. In this regard, **1N** possesses aromatic character in terms of the geometrical criterion. The phosphorus center adopts a trigonal pyramidal geometry with C−P−C bond angles of 91.2(13)−101.99(12)° ($\sum_{C-P-C}$ = 293.7°), and the P-phenyl group is located above the porphyrin π-plane as suggested by the NMR observations. These structural features imply that the porphyrin π-circuit does not involve the lone electron pair on the phosphorus. The core of **1N** provides a trapezoid cavity with $N_{22}-N_{24}$ and $P-N_{23}$ distances of 4.56 and 3.45 Å, respectively.

2. Optical and Electrochemical Properties. 2.1. Optical Property. The UV−vis absorption spectra of P,X,N_2-porphyrins **1X** and S,X,N_2-porphyrins **2X** (X = N, S) in CH_2Cl_2 are displayed in Figure 2.[30] The Soret bands of **1N** and **1S** appeared at λ_{ab} 431 and 440 nm (Table 3), respectively, which are red-shifted compared with those of **2N** (λ_{ab} 418 nm), **2S** (λ_{ab} 426 nm), and 5,10,15,20-tetraphenylporphyrin (H_2TPP, **10**) (λ_{ab} 411 nm).[2f,31] The longest Q-type transitions of **1N** (λ_{ab} 698 nm) and **1S** (λ_{ab} 718 nm) were also observed at longer wavelengths relative to those of **2N** (λ_{ab} 660 nm), **2S** (λ_{ab} 682 nm), and **10** (λ_{ab} 646 nm). Thus, the replacement of an N−H unit with a P-Ph unit shifts the Soret and Q bands to the longer wavelengths more strongly than does the replacement with a sulfur atom. The UV−vis absorption spectrum of **1N′** (Soret, λ_{ab} 431 nm; Q, λ_{ab} 692 nm) was quite similar to the spectrum recorded on **1N**. The S,X,N_2-porphyrins **2X** were found to be fluorescent, whereas the P,X,N_2-porphyrins **1X** were observed to be nonfluorescent.

TABLE 2. Selected Bond Lengths[a] and Distances (Å) in the Crystal Structures

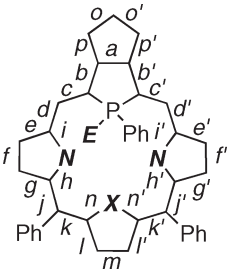

	compound		
	1N; 18π ***E***, ***X***, ***N*** = lone pair, NH, N	**6−O**; 22π ***E***, ***X***, ***N*** = O, N, NH	**7−O**; 20π ***E***, ***X***, ***N*** = O, S, NH
a	1.38	1.48	1.36
b (*b′*)	1.42	1.42	1.48
c (*c′*)	1.37	1.37	1.36
d (*d′*)	1.41	1.40	1.44
e (*e′*)	1.45	1.42	1.39
f (*f′*)	1.34	1.37	1.40
g (*g′*)	1.46	1.42	1.39
h (*h′*)	1.37	1.38	1.38
i (*i′*)	1.36	1.37	1.38
j (*j′*)	1.40	1.40	1.47
k (*k′*)	1.43	1.41	1.38
l (*l′*)	1.42	1.44	1.44
m	1.35	1.35	1.34
n (*n′*)	1.39	1.38	1.77
o (*o′*)	1.54	1.39	1.54
p (*p′*)	1.50	1.40	1.50
$N_{22}\cdots N_{24}$	4.56	4.47	4.69
$P\cdots X$	3.45	4.37	4.33
$P{=}O\cdots N_{22/24}$[b]		2.65	2.73

[a]Average values between *y* and *y′* (*y* denotes *b*−*l* and *n*−*p*). [b]Average values.

(30) In the previous reports (ref 23), we underestimated the molar absorbance coefficients (ε) for **1N** and **1S** owing to their gradual decomposition during sample preparation. Therefore, the samples for the UV−vis measurement of **1X** were prepared quickly under very weak light and remeasured. We checked that the spectra did not change under the measurement conditions.

(31) Delaere and Nguyen performed TD-DFT calculations on P,N_3-porphyrin **1N(H)-m** at the B3LYP/SV(P) level and predicted the red-shifts of the Soret and Q bands by 18−23 and 16−26 nm, respectively, as compared to those of N_4-porphyrin **10-m** (see ref 18).

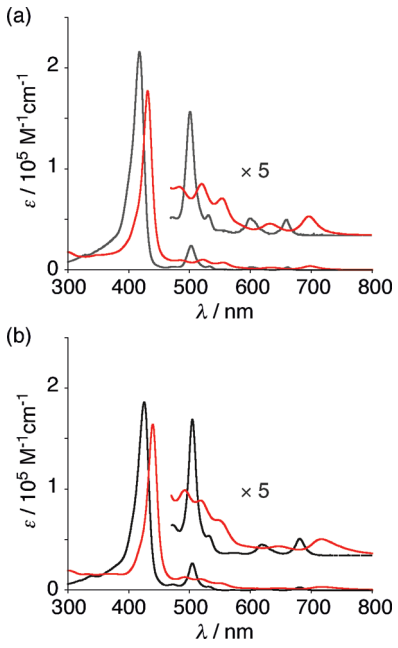

FIGURE 2. UV−vis absorption spectra of (a) **1N** (red) and **2N** (black) and (b) **1S** (red) and **2S** (black) in CH_2Cl_2.

TABLE 3. Absorption and Fluorescence Properties in CH_2Cl_2

	λ_{ab}, nm (ε, 10^3 M^{-1} cm^{-1})		
compound	Soret band	Q-band[b]	λ_{em}, nm[a] (Φ_F, %)
1N	431 (177)	698 (3.1)	nf[c]
1N′	431 (172)	692 (3.2)	nf[c]
1S	440 (164)	718 (3.1)	nf[c]
2N	418 (218)	660 (3.2)	665, 735 (0.94)[d]
2S	426 (188)	682 (3.4)	685, 760 (0.46)[e]
6−O	422 (42.1), 494 (77.2)	964 (2.5)	
6−S	424 (25.7), 485 (29.4)	750−1200 (sh)	
7−O	394 (66.1)	1130 (0.8)	

[a]Excited at 506 nm for **2N** and **2S**. [b]The longest absorption maxima. [c]Nonfluorescent. [d]Fluorescence quantum yield relative to Φ_F of **2S**. [e]Absolute fluorescence quantum yield determined by a calibrated integrating sphere system.

2.2. Electrochemical Property. Redox potentials of **1X** were measured by cyclic voltammetry (CV) and/or differential pulse voltammetry (DPV) and are compared with the potentials of **2X** and **10** (Figure 3; Figure S1 and Table S4 in Supporting Information). The electrochemical oxidation processes of **1N** and **1S** were found to be irreversible, and the first oxidation potentials ($E_{ox,1}$) of **1N** and **1S**, determined by DPV, were +0.38 and +0.45 V (vs Fc/Fc^+), respectively, both of which are more cathodic than $E_{ox,1}$ of **2N** (+0.62 V) and **2S** (+0.70 V). On the other hand, the electrochemical reduction of **1N** and **1S** occurred reversibly or quasi-reversibly, and the first reduction potentials ($E_{red,1}$) of **1N** and **1S** were −1.51 and −1.36 V, respectively, which are more anodic than those of **2N** (−1.56 V) and **2S** (−1.43 V). As a result, the differences in the redox potentials ($\Delta E = E_{ox,1} - E_{red,1}$) of **1N** (1.89 V) and **1S** (1.81 V) are significantly smaller than those of **2N** (2.18 V) and **2S** (2.13 V). The redox behavior of **1N′** ($E_{ox,1}$ = +0.41 V, $E_{red,1}$ = −1.52 V, ΔE = 1.93 V) is quite similar to that of **1N**. All of the P,X,N_2-porphyrins **1X** showed more negative $E_{ox,1}$ and more positive $E_{red,1}$ than H_2TPP **10** ($E_{ox,1}$ = +0.58 V, $E_{red,1}$ = −1.73 V, ΔE = 2.31 V).[2f]

3. DFT Calculations. To gain more insight into the structure, aromaticity, and optical and electrochemical properties of P,X,N_2-porphyrins **1X** and S,X,N_2-porphyrins **2X**, DFT calculations on a series of model compounds **1N-m**, **1S-m**, **1N(H)-m**,[32] **2N-m**, **10-m**, and **11-m** (Chart 4) at the B3LYP/6-311G(d,p) level were carried out. The optimized structures are shown in Figure 4, and selected bond lengths and distances are summarized in Table S2 in Supporting Information. The differences between the contiguous carbon(*meso*)−carbon(α) bond lengths (i.e., the absolute values of *d*−*c* and *k*−*j* in Table S2) of **1N-m** (0.01−0.03 Å) and **1S-m** (0.01−0.02 Å) are comparable to those of **10-m** (0.01 Å). In the structures of P,X,N_2-models **1X-m**, each phosphorus atom forms a pyramidal geometry ($\sum_{C-P-C}$ = 299.5° for both **1N-m** and **1S-m**), and the P-phenyl group is located above the macrocyclic plane (Figure 4a and b). These theoretical results are in good agreement with the experimental results (NMR and X-ray) observed for **1N** and **1S**. In contrast to the completely planar S,N_3-model **2N-m**, P,N_3-models **1N-m** and **1N(H)-m** possess slightly distorted π planes. The porphyrin π plane of **1S-m** deviates more than that of **1N-m**, probably as a result of the electrostatic repulsion between the two relatively large heteroatoms, P and S, making a dish-like macrocyclic platform with a slightly deeper bottom. The comparison of the optimized structure of the P-phenyl model **1N-m** with that of the P−H model **1N(H)-m** confirmed that the phenyl group attached to the phosphorus causes a slightly larger distortion of the macrocyclic framework (Figure 4a versus c; dihedral angles between the phosphole ring and the 24-atom mean plane for **1N-m** and **1N(H)-m** are 12.1° and 2.7°, respectively). However, the deviation caused by the introduction of the phenyl group is considerably smaller than that observed for N_4-porphyrins; the π planes of the N-alkyl and -aryl porphyrins have been reported to deviate substantially from planarity.[33] The N-phenyl pyrrole ring of **11-m** is tilted from the 24-atom mean plane with a dihedral angle of 34.9°, and the phenyl-bound nitrogen atom takes a flattened pyramidal geometry with the sum of the bond angles of $\sum_{C-N-C}$ = 342.9° (Figure 4f). This is because the core nitrogen atom in **11-m** aptly retains the sp^2 hybridization, even when it is phenylated.

Nucleus-independent chemical shifts (NICS) have been used as indices for evaluating the aromaticity of the porphyrin rings.[34] The NICS values at the center of the four heteroatoms of **1N-m** and **1S-m** were determined as −13.8 and −15.7 ppm, respectively (Table 4). The absolute NICS values of **1N-m** and **1S-m** are somewhat smaller than those of the N_4-porphyrin **10-m** (−16.5 ppm) and S,N_3-porphyrin **2N-m**

(32) In ref 18, Delaere and Nguyen calculated the optimized structure and orbital energies of **1N(H)-m** at the B3LYP/6-31G* and B3LYP/SV(P) levels, respectively. The orbital energies reported by these authors are as follows: −5.88 (HOMO−2), −5.50 (HOMO−1), −5.47 (HOMO), −2.69 (LUMO), and −2.44 eV (LUMO+1).

(33) (a) Lavallee, D. K.; Anderson, O. P. *J. Am. Chem. Soc.* **1982**, *104*, 4707–4708. (b) Kuila, D.; Lavallee, D. K. *J. Am. Chem. Soc.* **1984**, *106*, 448–450. (c) Aizawa, S.; Tsuda, Y.; Ito, Y.; Hatano, K.; Funahashi, S. *Inorg. Chem.* **1993**, *32*, 1119–1123.

(34) For example, see: (a) Cyrañski, M. K.; Krygowski, T. M.; Wisiorowski, M.; van Eikema Hommes, N. J. R.; Schleyer, P. von R. *Angew. Chem., Int. Ed.* **1998**, *37*, 177–180. (b) Furuta, H.; Maeda, H.; Osuka, A. *J. Org. Chem.* **2001**, *66*, 8563–8572.

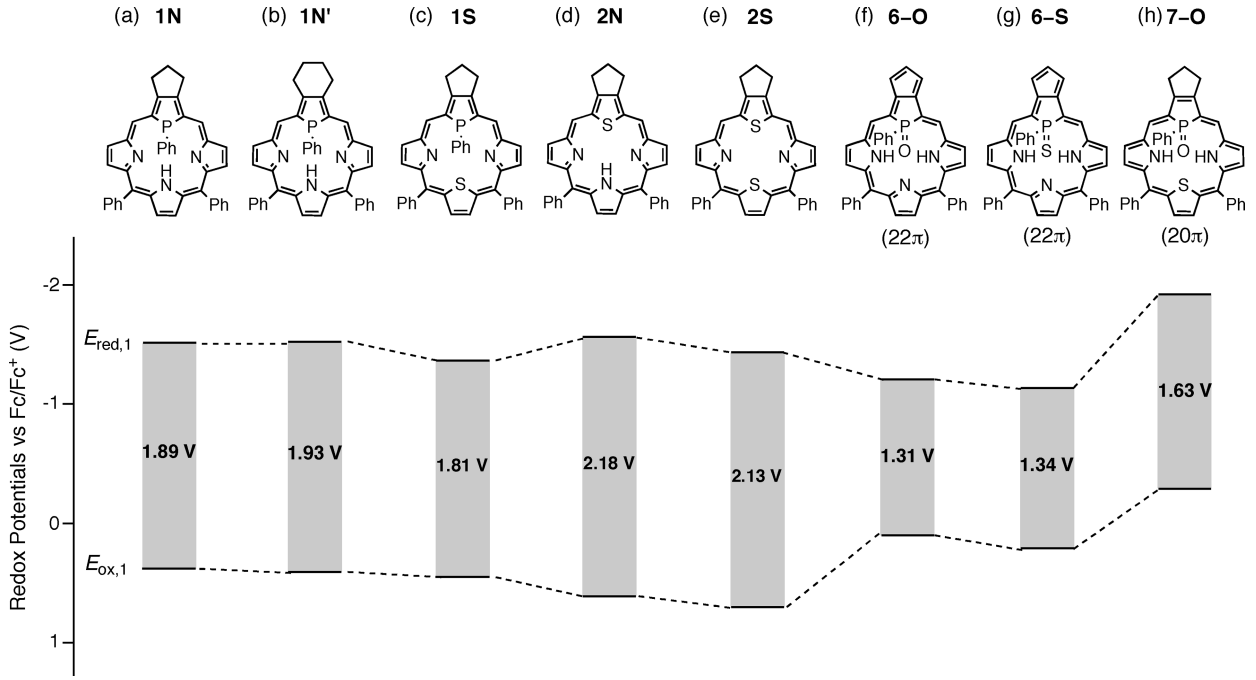

FIGURE 3. First oxidation ($E_{ox,1}$) and reduction ($E_{red,1}$) potentials for (a) **1N**, (b) **1N′**, (c) **1S**, (d) **2N**, (e) **2S**, (f) **6**−**O**, (g) **6**−**S**, and (h) **7**−**O**.

CHART 4. Model Compounds

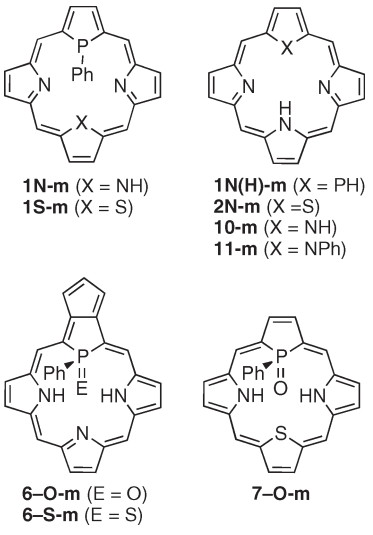

(−16.2 ppm) but are sufficiently large enough to maintain aromaticity. On the basis of these theoretical results, together with the above-mentioned experimental data, we can conclude that the inherent aromaticity is maintained in the P,X,N_2-porphyrin 18π systems.

The frontier orbitals of the model compounds are depicted in Figure 5. The replacement of a core nitrogen atom of porphyrin with a chalcogen atom is well-known to stabilize LUMOs more largely than HOMOs. This is commonly explained by the inductive or electron-withdrawing effect that the heteroatom has on the frontier orbitals.[1a,g] Indeed, in our calculations, HOMO and one of the nearly degenerated LUMOs of the S,N_3-model **2N-m** are stabilized by 0.10 and 0.18 eV, respectively, relative to those of the N_4-model **10-m**. As a result, the HOMO−LUMO gap of **2N-m** becomes narrower by 0.08 eV than that of **10-m**. The DFT calculations on the P−H model **1N(H)-m**[32] showed that the replacement of an N−H group with a P−H group stabilizes the HOMO and LUMO by 0.17 and 0.29 eV, respectively, and the HOMO−LUMO gap of **1N(H)-m** becomes narrower by 0.12 eV than that of **10-m**. Therefore, the core modification with phosphorus has more significant impacts on the frontier orbitals than that with sulfur.

Phosphaporphyrins contain three high-energy HOMOs due to the involvement of a lone electron pair and a substituent (Ph, H) at the phosphorus atom. In the P-Ph porphyrin **1N-m**, the lone electron pair orbital at the phosphorus effectively mixes into one of the two inherent HOMOs of porphyrin (the one that has large orbital coefficients at the core and *meso* positions), thus giving rise to significantly destabilized HOMO and HOMO-2 (by 0.17 and 0.33 eV) in comparison with those of **1N(H)-m**. Presumably, the $\sigma-\pi$ antibonding interaction between the P-C(Ph) σ orbital and the porphyrin π orbital in **1N-m** leads to the destabilization of these HOMOs. Similar orbital interactions appear in the P,S,N_2-porphyrin **1S-m**. The large contribution of the phosphorus lone pair to the HOMO explains the unique reactivity of **1X** (vide infra). As seen in Figure 5f, the HOMOs of **11-m** are destabilized by 0.07−0.14 eV relative to those of the N−H counterpart **10-m**, which is attributable to a steric factor rather than an orbital interaction.

Overall, the HOMO levels of **1N-m** (−5.42 eV) and **1S-m** (−5.39 eV) are comparable to the HOMO level of the N_4-porphyrin **10-m** (−5.42 eV), whereas the LUMO levels of **1N-m** (−2.78 eV) and **1S-m** (−2.90 eV) are largely stabilized by 0.28 and 0.40 eV relative to that of **10-m** (−2.50 eV). As a consequence, the HOMO−LUMO gaps of **1N-m** (2.64 eV) and **1S-m** (2.49 eV) are considerably smaller than the gap calculated for **10-m** (2.92 eV). These DFT results are in good agreement with the above-mentioned experimental results in that the core modification of porphyrin from the N-H unit or

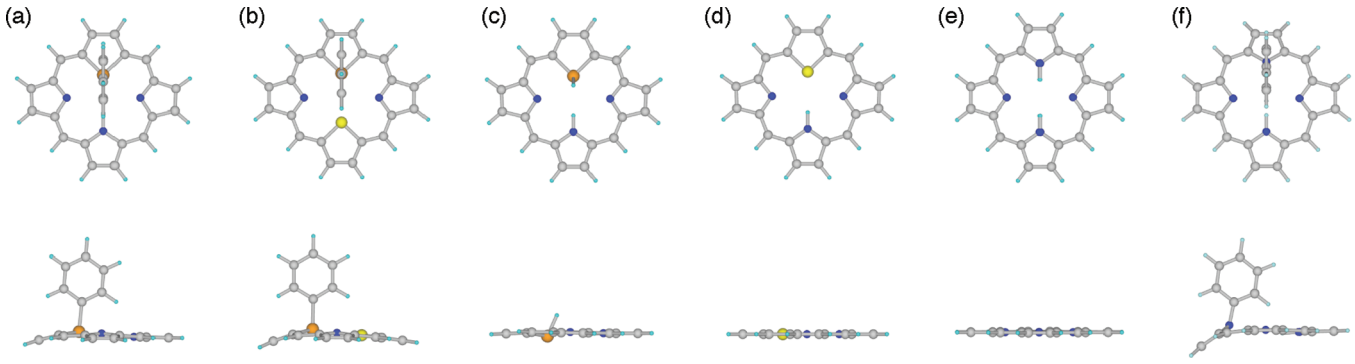

FIGURE 4. Top (upper) and side (lower) views of the optimized structures for (a) **1N-m**, (b) **1S-m**, (c) **1N(H)-m**, (d) **2N-m**, (e) **10-m**, and (f) **11-m**. The C, H, N, P, and S atoms are indicated as gray, light blue, blue, orange, and yellow balls, respectively.

TABLE 4. NICS Values for Model Compounds

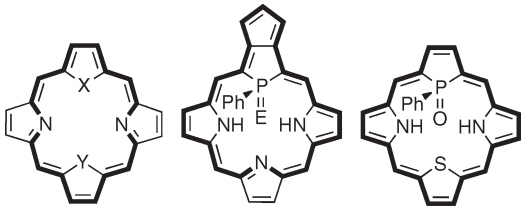

compound	NICS (ppm)
Type A (18π)	
1N-m (X = PPh, Y = NH)	−13.8[a]
1S-m (X = PPh, Y = S)	−15.7[a]
2N-m (X = S, Y = NH)	−16.2[a]
10-m (X,Y = NH)	−16.5[a]
Type B (22π)	
6−O-m (E = O)	−9.9[b]
6−S-m (E = S)	−8.8[b]
Type C (20π)	
7−O-m	2.4[b]

[a]Calculated at the center of the four heteroatoms. [b]Calculated at the center of the two facing nitrogen atoms.

the S atom to the P-Ph unit basically narrows the HOMO−LUMO gap.

4. P-Functionalized Phosphaporphyrins. 4.1. Chemical Functionalization of a Core Phosphorus Atom. The electronic structures of phosphole-containing π-conjugated systems are well-known to be effectively altered by the chemical functionalization of the phosphorus atom.[17] We anticipated that oxidation of the core phosphorus atom would produce new π systems with different electronic structures. Moreover, the formation of byproducts **6−O** and **7−O** suggested to us that the P-oxygenation pathway would be involved in the synthesis of **1X**. With these concepts in mind, we examined the reactions of **1N**, **1N′**, and **1S** with H_2O_2 (Scheme 3).

Initially, the reaction of the C_4-bridge type P,N_3-porphyrin **1N′** with H_2O_2 in $CDCl_3$ was monitored by ^{1}H NMR spectroscopy at several intervals (Figure 6a). After 5 min, **1N′** was consumed completely, and P-oxo P,N_3-porphyrin **1N′−O**[35] was formed in 94% NMR yield with a small amount (6%) of its tautomer **12′**. The structures of **1N′−O** and **12′** were characterized on the basis of only the NMR spectra because of their instability in solution. (For detailed ^{1}H NMR peak assignments of the intermediates presented in this section, see Figures S4 and S5 in Supporting Information.) The ^{31}P resonances of **1N′−O** (δ_p 21.8 ppm) and **12′** (δ_p 39.2 ppm) appeared at the significantly downfield region in the spectra when compared with the ^{31}P resonance of **1N′** (δ_p −32.6 ppm), supporting the notion that the phosphorus atom was oxygenated. The tautomer **12′** shows an asymmetric ^{1}H peak pattern with two NH protons (δ 13.8; 12.4), two *meso* protons (δ 5.60, d, $^3J_{P,H}$ = 25.8 Hz; δ 7.12, d, $^3J_{P,H}$ = 35.6 Hz), and an olefinic proton of the peripheral cyclohexene ring (δ 6.09, pseudo t, J = 4.0 Hz). Most of **1N′−O** was converted into **12′** within 60 min,[36] whereas **12′** slowly decomposed to afford a complex mixture after 3 h. Next, the reaction of the C_3-bridge type P,N_3-porphyrin **1N** with H_2O_2 was monitored (Figure 6b). Within 5 min, **1N** (δ_p −5.2 ppm) was quantitatively converted to P-oxo P,N_3-porphyrin **1N−O** (δ_p 36.4 ppm), which was then tautomerized into **12** (δ_p 48.2 ppm). The spectral features of **1N−O** and **12** are very close to those of **1N′−O** and **12′**. In contrast to the reaction of **1N′**, however, the mixture of **1N−O** and **12** was ultimately (after 3 h) transformed into **6−O**, which was isolated in 77% yield. Finally, the reaction of the P,S,N_2-porphyrin **1S** with H_2O_2 was monitored (Figure 6c). After 10 min, **1S** (δ_p 18.6 ppm) was consumed to generate two types of P-oxo porphyrins **1S−O** (δ_p 43.8 ppm) and **7−O** in 76% and 17% NMR yields, respectively. On standing the solution for 48 h, **1S−O** decomposed completely, while **7−O** was obtained as the sole isolated product in 16% yield. The above results imply that the P-oxidation of **1N** and **1S** is one of the most plausible pathways leading to **6−O** and **7−O** in Scheme 1.

From the viewpoint of the syntheses of **6−O** and **7−O**, it seemed convenient to oxidize the macrocyclic rings of **5N−O** and **5S−O**, which were readily available from the corresponding σ^3- P,X,N_2-porphyrinogens **5X** in high yields (for details, see Supporting Information). In this context, the reactions of **5X−O** with DDQ were examined (Scheme 4). To

(35) The peripheral and P-phenyl protons of **1X−O** (X = N, N′, S) are upfield-shifted and downfield-shifted, respectively, as compared with those of **1X** (X = N, N′, S), suggesting that **1X−O** form more deviated structures than **1X**. See, Table S5 in Supporting Information.

(36) This type of tautomerization from σ^4-phospholes to σ^4-phospholenes was reported for the C_4-bridge type 2,5-diarylphosphole-*P*-sulfides: Nyulászi, L.; Hollóczki, O.; Lescop, C.; Hissler, M.; Réau, R. *Org. Biomol. Chem.* **2006**, *4*, 996–998.

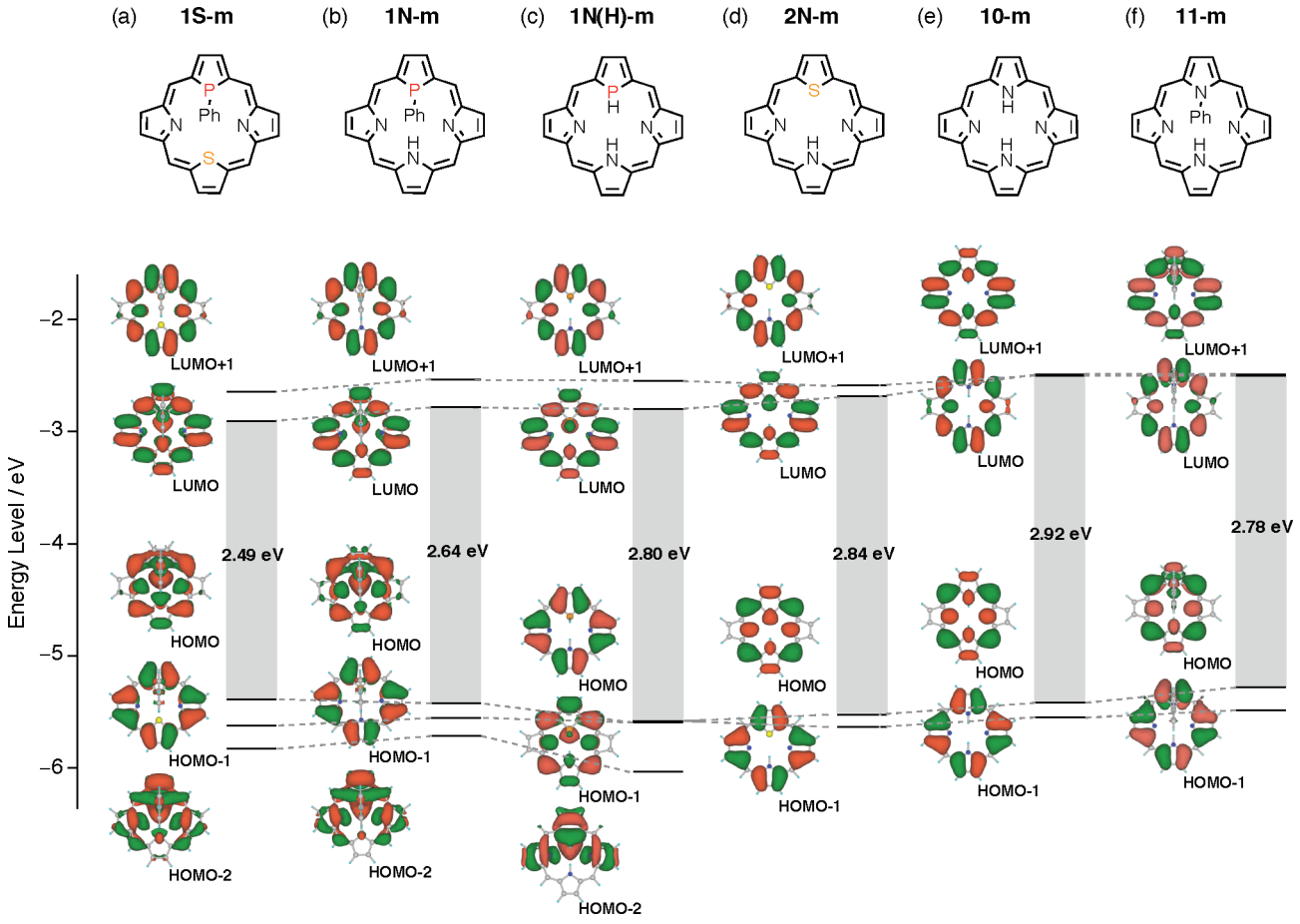

FIGURE 5. HOMOs and LUMOs of (a) **1S-m** (b) **1N-m**, (c) **1N(H)-m**, (d) **2N-m**, (e) **10-m**, and (f) **11-m**.

understand the substituent effects on the reactivity, DDQ oxidations of **5X**−**S** were also examined. Treatment of the P, N_3-porphyrinogens, **5N**−**O** and **5N**−**S**, with DDQ afforded **6**−**O** and **6**−**S** as the sole isolable products in 26% and 17% yields, respectively (Scheme 4). Hence, **5N**−**O** is also likely to be a precursor of **6**−**O** in the DDQ oxidation of **5N** depicted in Scheme 1. The overall yield of the conversion from **5N** to **6**−**O** via **5N**−**O** (25%) was better than the yield via **1N** (13%). The P-thioxo substituent in **5N**−**S** appreciably retarded the efficiency of the ring oxidation; however, the first P═S phosphaporphyrin **6**−**S** could be isolated as a dark brown solid. On the other hand, the DDQ oxidations of **5S**−**O** and **5S**−**S** gave complex mixtures, and the expected 20π porphyrins **7**−**O** and **7**−**S** were not obtained.[37]

As discussed below, both of the isolated P-oxo porphyrins **6**−**O** and **7**−**O** no longer possess ordinary 18π aromatic structures; the π system of **6**−**O** is extended to an unprecedented type of aromatic 22π system through the peripherally fused C_3-bridge, whereas **7**−**O** possesses an isophlorin-type antiaromatic 20π structure. Despite containing the isophlorin-type 20π structure, **7**−**O** is stable in air.[38] The formation of different types of π systems, **6**−**O** and **7**−**O**, can be reasonably explained by considering the following factors: (i) the steric congestion at the core, (ii) the electrostatic and hydrogen-bonding interactions among the core components, and (iii) the redox properties of the macrocyclic π systems (Scheme 5). Since the P-oxidation increases the steric congestion at the core, factor (i) is basically important for all the reactions in Scheme 3. Consequently, it is likely that factors (ii) and (iii) mainly determine the reaction pathways. In the simple P-oxygenated 18π porphyrins **1N**−**O** and **1S**−**O**, there must be electrostatic repulsion between the P═O moiety and the two adjacent nitrogen lone pairs at the core. By contrast, in **6**−**O** and **7**−**O**, there are two hydrogen bonds between the NH protons and the P═O moiety (vide infra). The reconstruction of the 18π structure of **1X**−**O** into the 22π (**6**−**O**) or 20π (**7**−**O**) structure arises to apparently relieve the "stress" and gain the attractive hydrogen-bonding interaction at the core. The intermediate **12**, in which the π circuit is interrupted at the peripheral five-membered ring, undergoes 2e-oxidation to gain the aromatic stabilization, giving **6**−**O** as the final product.[39] In contrast, in the case of **1S**−**O**, the formation of a tautomer like **13** is inhibited probably because such an intermediate is not stabilized

(37) DDQ oxidation of the P,O,N_2-type porphyrinogen-P-sulfide **5O**−**S** gave an unexpected N−C fused macrocyclic product (**S5**). For details, see Supporting Information.

(38) Isophlorins have an intrinsic nature to undergo 2e-oxidation (aromatization to 18π structure) under ambient conditions. See ref 6.

(39) On the basis of the time course of the reaction (Figures S8a and S9 in Supporting Information) and the result of an independent experiment (Figures S8b and S10 in Supporting Information), we presume that a coupled 2e-oxidation/2e-reduction between **12** and **1N**−**O** takes place to produce equimolar amounts of **6**−**O** (oxidized form) and an unidentified intermediate (reduced form; denoted as **IM** in Figures S8 and S9). Compound **IM** (not shown in Figure 6b) was slowly oxidized in situ to afford **6**−**O** (Scheme S4 in Supporting Information). For details, see Supporting Information.

SCHEME 3. Reactions of P,X,N_2-Porphyrins 1N′, 1N, and 1S with H_2O_2

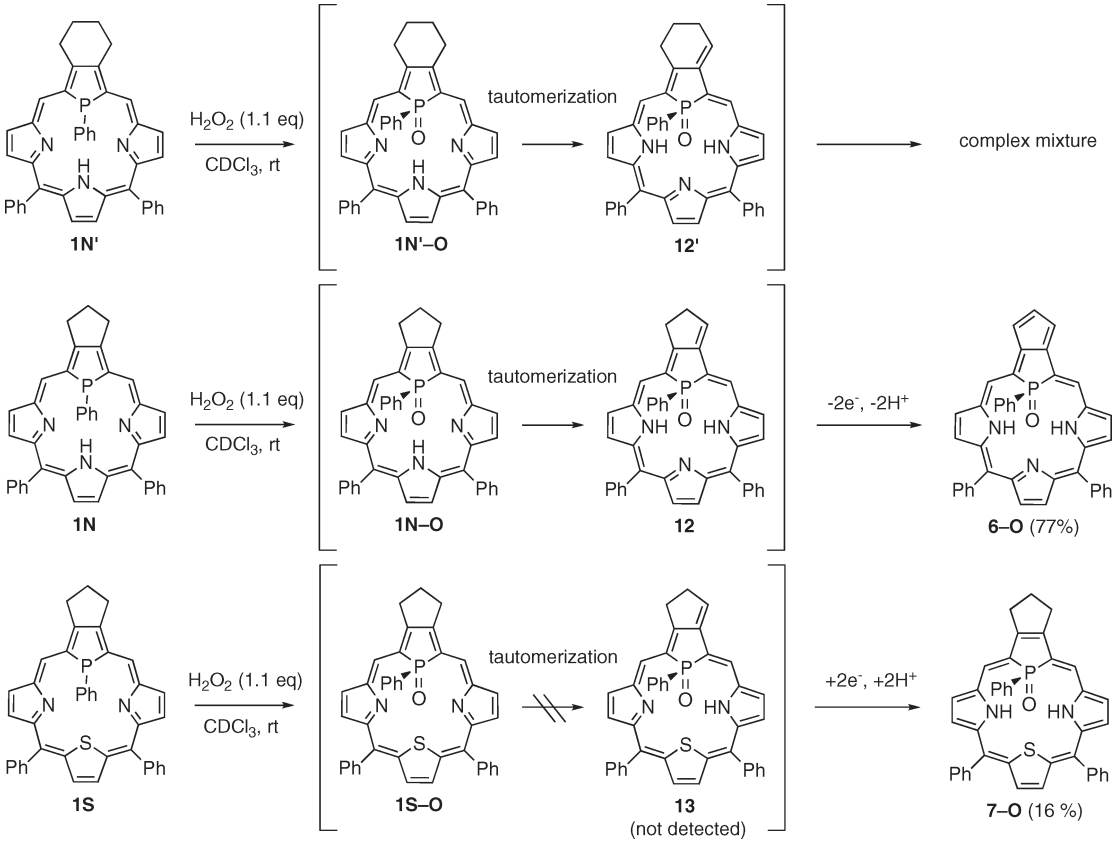

sufficiently by one hydrogen bond at the core (Scheme 3). Instead, the 2e-reduction of **1S**−**O** proceeds rapidly to afford the 20π porphyrin **7**−**O**,[40,41] and the overall reaction from **1S** to **7**−**O** is formally regarded as a hydration. It should be emphasized that the core phosphorus atom of **1N** and **1S** acts as a kind of switch, which realizes a dramatic alteration of the π-electronic structure by a simple chemical modification.[42]

4.2. Structures, Aromaticity, and Optical and Electrochemical Properties of P-Functionalized Phosphaporphyrins. Single crystals of **6**−**O** and **7**−**O** were grown from CH_2Cl_2−MeOH at room temperature (for **6**−**O**)[23b] or from CH_2Cl_2 at −10 °C (for **7**−**O**). Top and side views of **7**−**O** are depicted in Figure 7, and selected bond lengths and distances of **6**−**O** and **7**−**O** are summarized in Table 2. Unfortunately, we could not obtain high-quality single crystals of **6**−**S**. In the crystal structures of **6**−**O** and **7**−**O**, each core phosphorus atom adopts a tetrahedral geometry with C−P−C/C−P−O angles of 94.3(3)−107.5(2)°/108.1(3)−119.09(18)° and 94.3(3)−107.5(2)°/108.1(3)−119.09(18)°, respectively. To avoid the steric congestion at the core, the phosphole rings lean substantially outward. As a consequence, the phosphorus atom deviates from the 24-atom mean plane by 1.20 Å (for **6**−**O**) and 1.22 Å (for **7**−**O**), and the P−C(Ph) bond axis tilts against the mean plane by 114.5° (for **6**−**O**) and 115.1°(for **7**−**O**). These values are larger than those observed for P,N_3-porphyrin **1N** (0.34 Å and 82.5°), indicating that the π circuits in the P-oxo derivatives **6**−**O** and **7**−**O** are distorted considerably as compared with the 18π circuit of **1N**. The 22π aromaticity of **6**−**O** is well corroborated by the significantly diminished carbon−carbon bond length alternation through the 22π-circuit including the exocyclic C_3-bridge. The differences between the contiguous carbon(*meso*)−carbon(α) and carbon(C_3-bridge)−carbon(C_3-bridge) bond lengths of **6**−**O** (i.e., the absolute values of $d-c$ and $k-j$, and $o-o'$ in Table 2) are 0.00−0.03 and 0.00 Å, respectively. In contrast, notable bond length alternation is observed for **7**−**O**, in which the differences between the contiguous carbon(*meso*)−carbon(α) bond lengths are 0.07−0.09 Å. This indicates that the aromaticity is lost for the 20π-circuit of **7**−**O** (Table 2). The relatively short P═O···$N_{22/24}$ distances (2.65 Å for **6**−**O** and 2.73 Å for **7**−**O**) clearly display the presence of intramolecular hydrogen-bonds between the P-oxo group and the two adjacent NH protons.[43] This interaction is likely to play a crucial role in stabilizing the novel 22π and 20π systems.

(40) Deducing from the reduction potentials of **1S** ($E_{red,1}$ = −1.36 V, $E_{red,2}$ = −1.56 V), **1N** (−1.51 V, −1.74 V), and **1N′** (−1.52 V, −1.72 V), **1S**−**O** should have higher electron affinity than **1N**−**O** and **1N′**−**O**.

(41) On the basis of the time course of the reaction (Figures S8d and S11 in Supporting Information) and the result of an independent experiment (Figures S8e and S12 in Supporting Information), we presume that unreacted **1S** reduces **1S**−**O** to **7**−**O** and is transformed to **1S**−**O** (Scheme S5 in Supporting Information). Indeed, the addition of **1S** to a solution containing **1S**−**O** produces **7**−**O** quantitatively. For details, see Supporting Information.

(42) The reference S,N_3-porphyrin **2N** does not react with H_2O_2 even under more harsh conditions (ca. 100 equiv of H_2O_2, 24 h).

(43) The N···O distances for the NH···O hydrogen bonds in dimethylammonium hydrogen diphenyldiphosphonate were reported to be 2.75−2.77 Å: Courtney, B. H.; Juma, B. W. O.; Watkins, S. F.; Fronczek, F. R.; Stanley, G. G. *Acta Crystallogr.* **2006**, *C62*, o268–o270.

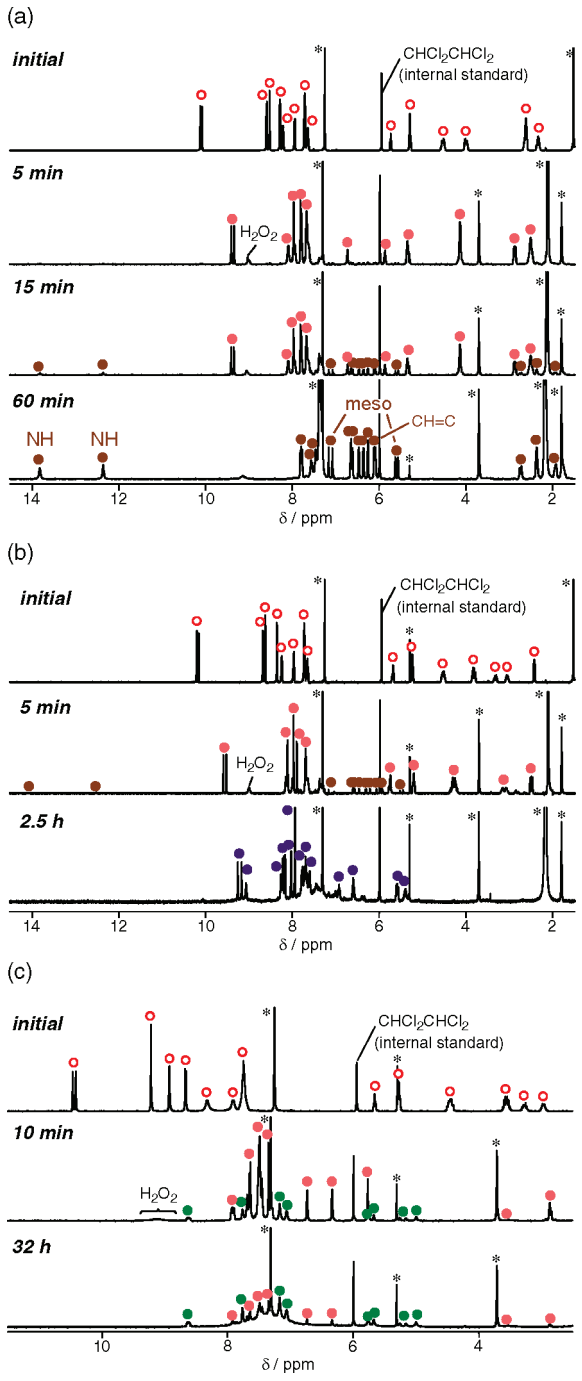

FIGURE 6. ^{1}H NMR monitoring experiments of the reactions between P,X,N_2-porphyrins (3.3 μmol) and H_2O_2 (30 wt %, 3.6 μmol) in $CDCl_3$/THF-d_8 (total 0.64 mL; v/v = 14/1) with 1,1,2,2-tetrachloroethane as an internal standard. (a) The reaction of **1N′** (open red circle); **1N′−O** (pink circle), **12′** (brown circle). (b) The reaction of **1N** (open red circle); **1N−O** (pink circle), **12** (brown circle), **6−O** (purple circle). (c) The reaction of **1S** (open red circle); **1S−O** (pink circle), **7−O** (green circle). Asterisk (*) indicates the peaks of residual solvents.

To obtain more information on the structures and the aromaticity of **6−O**, **6−S**, and **7−O**, DFT calculations on their model compounds **6−O-m**, **6−S-m**, and **7−O-m** (Chart 4) were performed at the level of B3LYP/6-311G(d, p). The optimized structures of these models are depicted in Figure 8, and selected bond lengths, distances, and angles are listed in Table S2 in Supporting Information. The bond parameters of the optimized structures of **6−O-m** and **7−O-m** are very close to those of the crystal structures of **6−O** and **7−O**. As shown in Figure 8, the phosphole ring of **6−S-m** is tilted more than the phosphole rings of **6−O-m** and **7−O-m** to accommodate the bulky P=S moiety in the core.[44] The P=S···$N_{22/24}$ distances (each 3.13 Å) calculated for **6−S-m** suggest the presence of intramolecular hydrogen-bonding interaction between the P-thioxo group and the two adjacent NH protons.[45]

In the HR-FAB-MS spectra, **6−O**, **6−S**, and **7−O** clearly show parent ion peaks (M^+) at m/z 609.1975 (calcd for $C_{41}H_{28}N_3OP$, 609.1975 for **6−O**), 625.1742 (calcd for $C_{41}H_{28}N_3PS$, 625.1738 for **6−S**), and 630.1895 (calcd for $C_{41}H_{31}N_2OPS$, 630.1895 for **7−O**). In the ^{1}H NMR spectrum of **6−O**, *meso*, pyrrole-β, NH, and P-phenyl protons appear at δ 9.21 (d, $^3J_{P,H}$ = 35.6 Hz), 7.94−8.19, 5.40, and 5.60−6.92 ppm, respectively (Figure 1c). Additionally, the peripheral protons that originate from a C_3-bridge of the phosphole backbone are observed at δ 8.16 (d, J = 3.9 Hz, 2H) and 9.06 (dt, J = 3.9 Hz, $^5J_{P,H}$ = 5.4 Hz, 1H) ppm, indicating that the π-circuit goes through the five-membered fused ring in **6−O**. The ^{31}P peak of **6−O** appears at δ 28.6 ppm, which is considerably shielded when compared with that of the P-oxo P,N_3-porphyrinogen **5N−O** (δ 59.2−59.6 ppm, Table S1 in Supporting Information). These NMR data obviously reflect diatropic ring-current effects induced by the aromatic 22π circuit of **6−O**; however, both shielding and deshielding effects are somewhat diminished in comparison with **1N**. This reduction in shielding and deshielding is due to the deviated structure of **6−O**. The ^{1}H NMR spectrum of **6−S** (Figure 1d) is quite different from that of **6−O**. The C_3-bridge protons appear at δ 3.80 (d, J = 3.4 Hz, 2H) and 5.70 (dt, J = 3.4 Hz, $^5J_{P,H}$ = 5.4 Hz, 1H) ppm, respectively, which are significantly upfield-shifted by 4.36 and 3.36 ppm from those of **6−O**. In contrast, the P-phenyl protons of **6−S** (δ 7.5−8.23 ppm) are downfield-shifted by 0.6−2.63 ppm from those of **6−O**. As mentioned above, the phosphole ring of **6−S** (**6−S-m**) is considerably tilted from the mean π plane and the P-phenyl group leans outward from the cavity. As a result of this large deviation, the C_3-bridge and P-Ph moieties in **6−S** are located in regions where the diatropic ring-current effect is weak. However, the highly distorted 22π circuit of **6−S** retains moderate aromaticity; significant upfield shifts ($\Delta\delta$ = 0.84−0.99 ppm) are seen for the pyrrole-β protons of **6−S** as compared with those of the corresponding calixphyrin **8N−S**[24b,c] (Table 1). Indeed, the NICS value at the center of the two facing nitrogen atoms of **6−S-m** (−8.8) is only slightly positive relative to that of **6−O-m** (−9.9) (Table 4).

In contrast to **6−E** (E = O, S), **7−O** displays weakly paratropic ring current effects in the ^{1}H NMR spectrum (Figure 1e). Specifically, the pyrrole-β and P-phenyl protons of **7−O** appear at δ 4.99−5.68 and 7.75−8.64 ppm, respectively,

(44) The phosphorus atom deviates from the respective mean π planes by 0.30 Å (for **1N-m**), 1.16 Å (for **6−O-m**), 1.35 Å (for **6−S-m**), and 1.24 Å (for **7−O-m**), and the P−C(Ph) bond axis slants against the plane by 84.7° (for **1N-m**), 116.4° (for **6−O-m**), 135.2° (for **6−S-m**), and 113.9° (for **7−O-m**).

(45) The N···S distances for the NH···S hydrogen bonds in silver−antimony sulfides were reported to be 3.20−3.65 Å: Vaqueiro, P.; Chippindale, A. M.; Cowley, A. R.; Powell, A. V. *Inorg. Chem.* **2003**, *42*, 7846–7851.

SCHEME 4. DDQ Oxidation of P-Functionalized Porphyrinogens 5N−O, 5N−S, 5S−O, and 5S−S

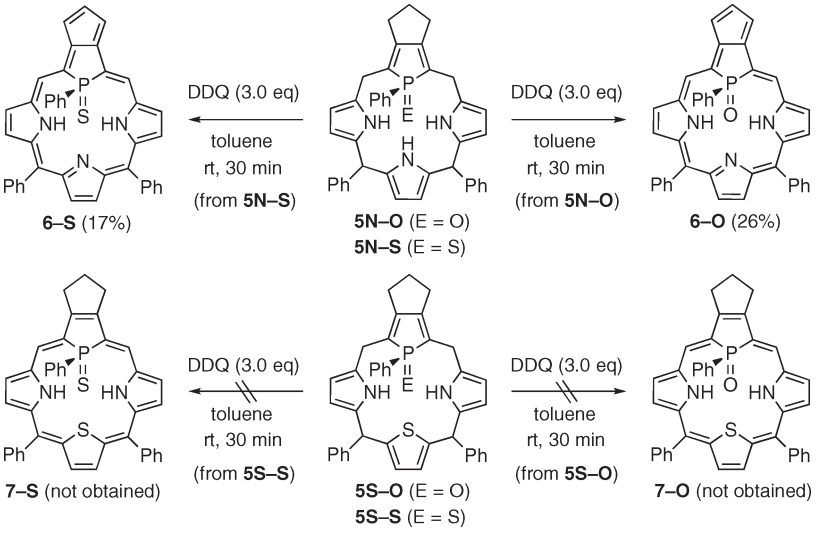

SCHEME 5. Reconstruction of π Systems via P-Oxidation

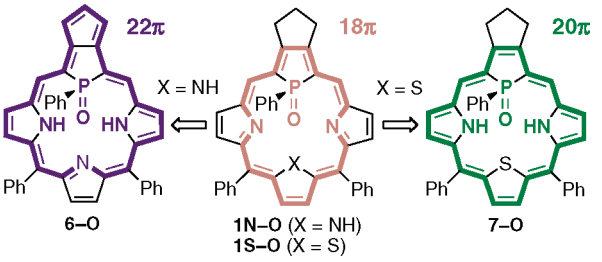

which are slightly upfield shifted ($\Delta\delta$ = −0.35 to −0.97 ppm) or downfield shifted ($\Delta\delta$ = 0.41−0.69 ppm) when compared with the chemical shifts of the protons in the corresponding calixphyrin **14**[24b,c] (Chart 3 and Table 1). Small, positive NICS values (+2.4) at the center of **7−O-m** support that **7−O** has weak antiaromaticity in terms of magnetic criterion (Table 4).

In the UV−vis absorption spectra of **6−E** (E = O, S), split Soret-like bands (**6−O**, λ_{ab} 422 and 494 nm; **6−S**, λ_{ab} 424 and 485 nm) and a remarkably broad, low-energy band reaching into a near-infrared region were observed (Figure 9a and Table 3). The absorption coefficients of **6−S** are considerably smaller than that of **6−O**. This is presumably due to the structural deviation of **6−S**. The UV−vis absorption spectrum of **7−O** shows a broad Soret-like band at the high-energy region (λ_{ab} 394 nm) and no detectable Q bands, which is characteristic of highly ruffled, nonaromatic 4nπ porphyrinoids (Figure 9b).[25,46]

The electrochemical oxidation processes of **6−E** (E = O, S) were found to be irreversible, whereas the reduction processes were reversible or quasi-reversible (Figure S2 in Supporting Information). The first oxidation and reduction potentials of **6−O** ($E_{ox,1}$ = +0.10 V; $E_{red,1}$ = −1.21 V, vs Fc/Fc$^+$) and **6−S** ($E_{ox,1}$ = +0.21 V; $E_{red,1}$ = −1.13 V, vs Fc/Fc$^+$) are more cathodic and more anodic as compared

(46) (a) Yamamoto, Y.; Yamamoto, A.; Furuta, S.-y.; Horie, M.; Kodama, M.; Sato, W.; Akiba, K.-y.; Tsuzuki, S.; Uchimaru, T.; Hashizume, D.; Iwasaki, F. *J. Am. Chem. Soc.* **2005**, *127*, 14540–14541. (b) Cissell, J. A.; Vaid, T. P.; Yap, G. P. A. *Org. Lett.* **2006**, *8*, 2401–2404. (c) Liu, C.; Shen, D.-M.; Chen, Q.-Y. *J. Am. Chem. Soc.* **2007**, *129*, 5814–5815.

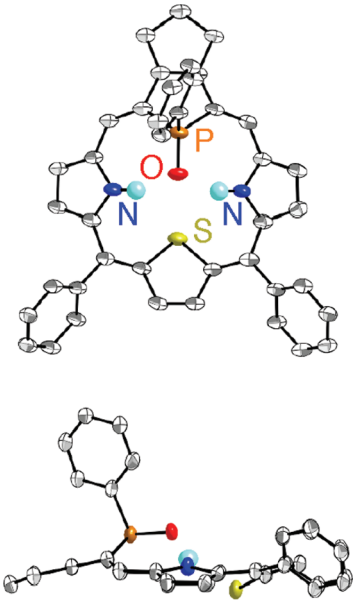

FIGURE 7. Top (upper) and side (lower) views of **7−O** (30% probability ellipsoids). Hydrogen atoms (except for NH) and solvent molecules are omitted for clarity.

with the respective values of **1N** (Figure 3). As a result, this yields very small HOMO−LUMO gaps for **6−O** (ΔE = 1.31 V) and **6−S** (ΔE = 1.34 V) in comparison with **1N** (ΔE = 1.89 V). The electrochemical oxidation processes of **7−O** occurred reversibly at −0.29 and +0.02 V (vs Fc/Fc$^+$). The first oxidation and reduction potentials of **7−O** ($E_{ox,1}$ = −0.29 V; $E_{red,1}$ = −1.92 V, vs Fc/Fc$^+$) are considerably cathodically shifted when compared with the respective values of **1S** (Figure 3), which exhibits the isophlorin character of the π system of **7−O**. As a whole, the calculated HOMO and LUMO levels of the model compounds **6−O-m** (−4.96 and −3.03 eV), **6−S-m** (−5.00 and −3.12 eV), and **7−O-m** (−4.47 and −2.41 eV) are in good agreement with the observed redox potentials (Figure S3 in Supporting Information). It is noteworthy that the HOMO−LUMO gaps of the P-oxidized derivatives **6−O**, **6−S**, and **7−O** are much narrower than those

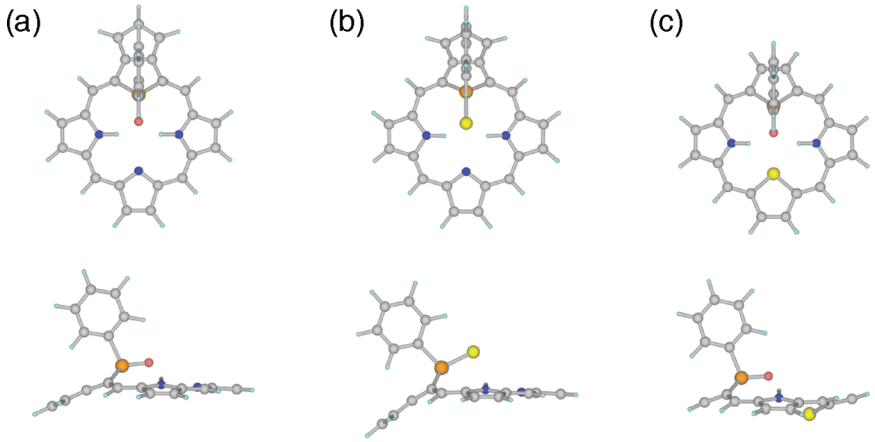

FIGURE 8. Top (upper) and side (lower) views of the optimized structures for (a) **6**−**O-m**, (b) **6**−**S-m**, and (c) **7**−**O-m**: gray (C), light blue (H), blue (N), red (O), orange (P), yellow (S).

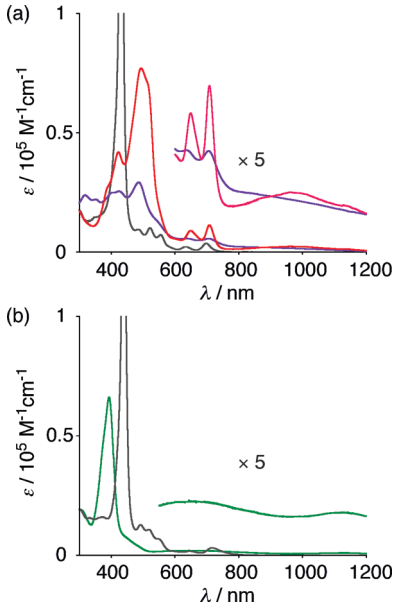

FIGURE 9. UV−vis absorption spectra of (a) **6**−**O** (reddish-purple) and **6**−**S** (bluish-purple) and (b) **7**−**O** (green) in CH_2Cl_2. The spectra of corresponding 18π porphyrins **1N** and **1S** are shown by a black line in each spectrum.

of the 18π σ^3-P,X,N_2 porphyrins **1X**. Most importantly, the optical and electrochemical properties of the P,X,N_2-porphyrin systems are readily tunable by simple P-oxidation reactions.

5. Concluding Remarks. We have successfully prepared 18π P,X,N_2-porphyrins **1N**, **1N′**, and **1S** via an acid-promoted [3 + 1] condensation approach using phosphatripyrranes and 2,5-bis-[hydroxy(phenyl)methyl]heteroles. Both experimental (NMR, UV−vis, and X-ray) and theoretical (DFT calculations) results have revealed that these P,X,N_2-porphyrins possess reasonably high aromaticity that stem from the slightly deviated 18π-annulene circuit. The UV−vis and CV/DPV measurements as well as the DFT calculations have also revealed that these P,X,N_2-porphyrins possess considerably narrow HOMO−LUMO gaps. It is of particular interest that the simple P-oxygenation of σ^3-P,X,N_2-porphyrins with H_2O_2 causes unprecedented types of π-reconstruction from 18π into peripherally extended 22π or isophlorin-type 20π circuits. Notably, the reaction modes and the structures of the resulting P-oxygenated porphyrins strongly depend on the combination of the core heteroatoms and the structure of the peripherally fused carbocycles. The present results demonstrate for the first time that the introduction of a phosphorus atom into the core is a highly promising methodology to modify the fundamental properties and reactivities of porphyrin π systems.

Experimental Section

X-ray Crystallography. Single crystals suitable for X-ray analysis were grown from CH_2Cl_2−MeOH (for **1N**, **6**−**O**, and **S5**) or from CH_2Cl_2 (for **7**−**O**). X-ray crystallographic measurements were made on a Rigaku Saturn CCD area detector with graphite monochromated Mo Kα radiation (0.71070 Å) at −150 °C. The data were corrected for Lorentz and polarization effects. The structures were solved by using direct methods[47] and refined by full-matrix least-squares techniques against F^2 using SHELXL-97.[48] The non-hydrogen atoms were refined anisotropically, and hydrogen atoms were refined using the rigid model. The CIF files of **1N** and **6**−**O** were deposited as Supporting Information files in ref 23b (**1N** and **6**−**O** correspond to **7** and **8**, respectively, in ref 23b).

DFT Calculations on Model Compounds. The structures of model compounds were optimized using DFT. The basis set used was 6-311G(d,p).[49] The functionals of DFT was the Becke 1988 exchange and Lee−Yang−Parr correlation functionals (B3LYP).[50] The NICS values[51] were calculated at the Hartree−Fock level with gauge-including atomic orbitals (GIAOs) at the DFT optimized structures. The basis set used in the NICS value computations was 6-31+G(d).[52] All

(47) SIR92: Altomare, A.; Cascarano, G.; Giacovazzo, C.; Guagliardi, A.; Burla, M.; Polidori, G.; Camalli, M. *J. Appl. Crystallogr.* **1994**, *27*, 435−436.
(48) Sheldrick, G. M. *SHELXL-97*; University of Göttingen: Germany, 1997.
(49) (a) Krishnan, R.; Binkley, J. S.; Seeger, R.; Pople, J. A. *J. Chem. Phys.* **1980**, *72*, 650–654. (b) McLean, A. D.; Chandler, G. S. *J. Chem. Phys.* **1980**, *72*, 5639–5648.
(50) (a) Becke, A. D. *J. Chem. Phys.* **1988**, *98*, 5648–5652. (b) Lee, C.; Yang, W.; Parr, R. G. *Phys. Rev. B* **1988**, *37*, 785–789.
(51) Schleyer, P. v. R.; Maerker, C.; Dransfeld, A.; Jiao, H.; van Eikema Hommes, N. J. R. *J. Am. Chem. Soc.* **1996**, *118*, 6317–6318.
(52) (a) Hehre, W. J.; Ditchfield, R.; Pople, J. A. *J. Chem. Phys.* **1972**, *56*, 2257–2261. (b) Francl, M. M.; Pietro, W. J.; Hehre, W. J.; Binkley, J. S.; DeFrees, D. J.; Pople, J. A.; Gordon, M. S. *J. Chem. Phys.* **1982**, *77*, 3654–3665. (c) Clark, T.; Chandrasekhar, J.; Spitznagel, G. W.; Schleyer, P. von R. *J. Comput. Chem.* **1983**, *4*, 294–301.
(53) Pople, J. A. et al. *Gaussian 03*; Gaussian, Inc.: Pittsburgh PA, 2003. For a full list of the authors, see Supporting Information.

calculations were carried out using the Gaussian 03 suite of programs.[53] In the optimized structures of model compounds except for **1S-m**, the P-phenyl group is parallel to the P−X axis (X = NH, S). In the optimized structure of **1S-m**, the P-phenyl ring is found to be vertical to the P−S axis.[23a] However, the difference in energy between the optimized structure and the structure in which the P-phenyl ring is rotated by 90° (i.e., the P-phenyl ring is parallel to the P−S axis) is very small (1.87 kcal mol^{-1}). Thus, the binding for the P-phenyl ring rotation is considered to be very weak. In this paper, the parallel structure was used for discussion.

Acknowledgment. This work was supported by a Grant-in-Aid for Science Research on Priority Areas (no. 20038039) from the Ministry of Education, Culture, Sports, Science and Technology of Japan. We thank Prof. Takahiro Sasamori, Prof. Norihiro Tokitoh (Kyoto University), and Prof. Hidemitsu Uno (Ehime University) for the analysis of X-ray crystallography. We also thank Dr. Kengo Suzuki (Hamamatsu Photonics K.K.) for the measurement of absolute fluorescence quantum yields of **2S**. T.N. thanks a JSPS fellowship for young scientists.

Supporting Information Available: Experimental details and characterization data, ^{1}H and ^{13}C NMR charts for new compounds, CIF files for **7**−**O** and **S5**, Cartesian coordinates and energies of B3LYP/6-311G(d,p) geometry optimized structures for model compounds, and complete ref 53. This material is available free of charge via the Internet at http://pubs.acs.org.